REDOX-ACTIVE ORGANIC MOLECULE FUNCTIONALIZED GRAPHENE ELECTRODES FOR HIGH-POWER ENERGY STORAGE APPLICATIONS

A Dissertation
Presented to
The Academic Faculty

by

Siyao Cai

In Partial Fulfillment
of the Requirements for the Degree
Master's in science in the
George W. Woodruff School of Mechanical Engineering

Georgia Institute of Technology
August 2018

REDOX-ACTIVE ORGANIC MOLECULE FUNCTIONALIZED GRAPHENE ELECTRODES FOR HIGH-POWER ENERGY STORAGE APPLICATIONS

Approved by:

Dr. Seung Woo Lee, Advisor
School of Mechanical Engineering
Georgia Institute of Technology

Dr. Hailong Chen
School of Mechanical Engineering
Georgia Institute of Technology

Dr. Peter Hesketh
School of Mechanical Engineering
Georgia Institute of Technology

Date Approved: [May 8th, 2018]

[To the students of the Georgia Institute of Technology]

ACKNOWLEDGEMENTS

I wish to thank my advisor, Professor Seung Woo Lee, for his guidance and encouragement during pursing my master's degree. I sincerely appreciate Prof. Lee's support on my research. He encouraged me to explore different topics in Electrochemistry during pursing my master's degree to gain an all-around understanding of different Electrochemical energy storage devices and materials. During the past semesters, I was given the chance to generate researches ideas and design experiments to study the problems. The independent research skills I developed Prof. Lee's Lab will be beneficial for my future career. I would also thank my committee members, for your insightful comments on my research.

I would also thank other members from Prof. Lee's Lab, Dr. Tianyuan Liu, Mr. Byeongyong Lee, Dr. Jinho Park, Dr. Yongmin Ko, Dr. Myeongjin Kim, Mr. Michael Lee, Mr. Hoyoung Lee and Mr. Jong Ha. I learned a lot from my colleagues and I really enjoy working with them. Their suggestions were very helpful for my research. Also, I would like to express my thanks to my friends, Jiankai Zhang, Mohammadreza Nazemi, Xuetian Ma, Dr. Jianing Wu and Daniel Moreno for their suggestions on my research and career.

Financial support of my research was provided by Prof. Lee's startup fund from the Georgia Institute of Technology and George. W. Woodruff school of Mechanical Engineering Graduate Teaching Assistantship.

Lastly, I would like to thank my parents and my wife from the bottom of my heart for their supports and sacrifices, without their love and encouragement, I could not be here.

TABLE OF CONTENTS

LIST OF TABLES

LIST OF FIGURES

LIST OF SYMBOLS AND ABBREVIATIONS

AC	Activated Carbon
CNT	Carbon Nanotube
CHA	Chloranilic Acid
CV	Cyclic Voltammetry
DMQ	2,5-Dimethoxy-1,4-benzoquinone
DHQ	2,5-Dihydroxy-1,4-benzoquinone
EC	Electrochemical Capacitor
EDLC	Electrical Double Layer Capacitor
EIS	Electrochemical Impedance Spectroscopy
GO	Graphene Oxide
GH	Graphene Hydrogel
ICE	Internal Combustion Engine
LIB	Lithium-ion Battery
PVA	Polyvinyl-Alcohol
rGO	Reduced Graphene Oxide
SEM	Scanning Electron Microscope
THQ	Tetrahydroxyl-1,4-benzoquinone
XQ	p-xyloquinone
XPS	X-ray Photoelectron Spectroscopy
XRD	X-ray Diffraction

SUMMARY

Electrochemical energy storage devices are critical to the development of Electric Vehicles and sustainable transportation. Electrochemical Capacitor (EC), also known as the supercapacitor or ultracapacitor, is one of the potential energy sources for Electric Vehicles and Hybrid Electric Vehicles due to its high-power density and excellent cycling stability. However, ECs have low energy density due to the surface charge storage mechanism.[1] The ECs initially attracted attention for its potential on the short-term pulse applications. Recent years, due to the development of carbon-based energy storage materials, the energy density of ECs have been increased.[2, 3] Lithium-ion Battery (LIB) is another promising energy storage device, which provides high energy density but relatively low power density and cycling stability. The low power density is caused by the charge storage mechanism of LIB and the low cycling stability is mainly caused by the degradation of the anode during charging and discharging process. The insertion of Li^+ ions into the anode leads to a significant volume change of the anode and result in the pulverization of the anode. Carbon-based materials such as Carbon Nanotube (CNT), Activated Carbon (AC) and Graphene are widely used as the electrode materials for energy storage devices like ECs or LIBs due to their high electrical conductivity, large surface area and low cost.[4, 5] Tremendous efforts have been put into the electrode materials research for high-performance energy storage devices.[6]

In this thesis, we demonstrated the possibility of bridging the gap between the electrochemical capacitor and the LIBs with self-assembled redox-active organic molecule functionalized graphene electrode. Firstly, tetrahydroxyl-1,4-benzoquinone (THQ) was

introduced as reducing agent and functionalization agent simultaneously during the synthesis of the functionalized graphene electrode. The THQ functionalized electrode was tested in both aqueous and gel electrolyte, all showing great specific capacitance, 409 F/g in 1 M H_2SO_4 aqueous electrolyte at 1 A/g; 125 F/g in 1 M Li_2SO_4 aqueous electrolyte at 1 A/g and 315 F/g in H_2SO_4-PVA gel electrolyte at 1 A/g. The electrode showed around 70% capacitance retention after 5000 cycles in H_2SO_4-PVA gel electrolyte at 5 A/g, while only maintained 35% of its initial capacitance in aqueous electrolytes after 5000 cycles.

In the second half of this thesis, several quinone group molecules were introduced as functionalization agent of the hydrothermal reaction of GO, forming redox-active molecule functionalized electrodes. The electrodes were characterized and tested to determine their 3D microstructure and electrochemical performance. The 2,5-Dihydroxy-1,4-benzoquinone (DHQ) functionalized electrode showed excellent performance in the electrochemical testing, exhibiting a specific capacitance of 511 F/g in 1 M H_2SO_4 aqueous electrolyte at 1 A/g, which is almost three times higher than the specific capacitance of the reduced graphene oxide (rGO) electrode. The excellent performance is accredited to the joint contribution of its unique 3D microstructure and the oxygen functional group integrated onto the graphene surface during the hydrothermal reaction. The DHQ functionalized electrode also exhibits a great cycling stability, stabilized at ~90% of its initial capacitance after 2000 cycles at 50 mV/s scan rate. This is because of the high reaction temperature leading to the robust integration of the oxygen functional group on the surface of the graphene layer.

More works will be continued in the future to further investigate the quinone group molecules functionalized electrodes and the role of the methoxy group, methyl group and

hydroxy group in the synthesis process and the electrochemical tests. Other applications of the functionalized electrode will also be explored including electrodes for yarn supercapacitors as the energy source for wearable devices. The quinone group molecule functionalized electrodes will also be tested as electrodes of LIB.

CHAPTER 1. INTRODUCTION

1.1 Motivation

Due to the limitations of Internal Combustion Engines (ICEs) and the regulations on conventional vehicles. The electrification of vehicles has been an irreversible trend for today's ground transportation. With the rapid development of the electrical vehicles and the portable electronic devices, the demand for energy storage devices with high energy density, high power density and long cycling life has significantly increased.[7] Electrochemical energy storage devices have attracted considerable attention over the past decades. Among the devices, Lithium-ion battery (LIB) and Electrochemical capacitors (ECs) have attracted the most attention. The LIB was first commercialized by Sony in 1991, with a gravimetric energy density of 120-150 W h/kg.[8] Both the ECs and the rechargeable batteries have the similar configuration, which consists of two electrodes (cathode vs. anode or positive vs. negative), a polymer separator that separates the anode and the cathode from physical connection and electrolyte that allows the ion transfer between the two electrodes. However, the charge storage mechanism for EC and LIB are different.[9, 10]

1.2 Electrochemical Energy Storage Devices

1.2.1 Electrochemical Capacitor

EC, also called as supercapacitor, is one of the most studied electrochemical energy storage devices. The configuration of EC is shown in **Figure 1.1**, where the two electrodes are separated by a porous polymer film. The plate shown in Figure 1.1 is working as a current collector that connect both electrodes to the external appliance.

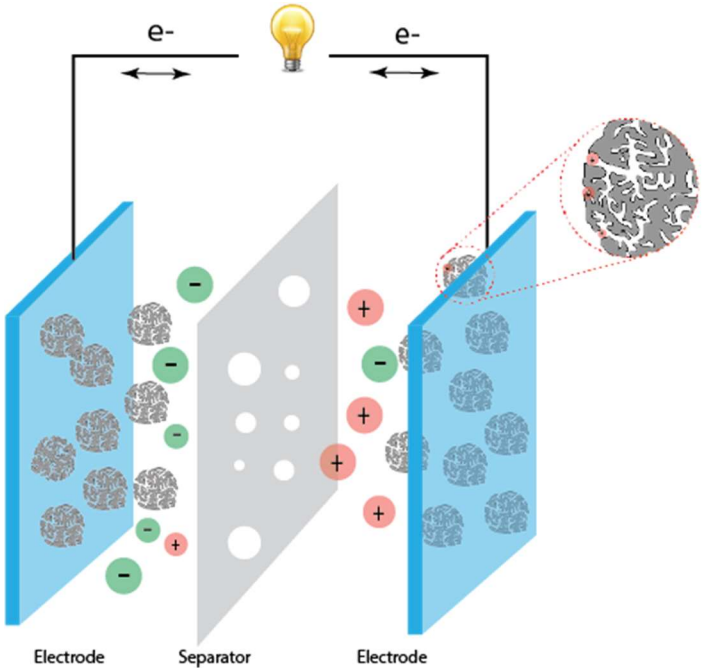

Figure 1.1 Schematic of Electrochemical Capacitor

Compared to LIBs, ECs have higher power density and better cycling stability.[11] There are two types of ECs, Electrical Double Layer Capacitor (EDLC) and the Pseudo-capacitor. These two types of ECs have different charge storage mechanisms. For EDLC, the charges are mainly stored on the surface of the electrode.[12] During the charging process, the charges accumulate to the surface of the electrodes forming electrical double layers at the interface between the electrode and electrolyte. During the discharge process, the charges are desorbed from the surface of the electrodes (**Figure 1.1**). Thus, EDLC has much higher power density compared to LIB and other energy storage devices. However,

since the charges are mostly stored on the surface of the electrode, the electrochemical performance of EDLC mainly depends on the surface area of the electrode, pore size and electrolyte ions. Activated Carbon (AC), Carbon Nanotube (CNT) and Graphene are the most studied materials for EDLC electrode materials due to their high surface area, large pore size and relatively low price.[3, 5, 6] For pseudocapacitor, the charges are stored via faradic reactions that involve fast and reversible redox reactions between the electrolyte and the active materials.[13] Popular active materials for pseudocapacitor include the metal oxide and polymers.[14, 15] **Figure 1.2** shows the specific power vs. the specific energy for various energy storage devices.[16]

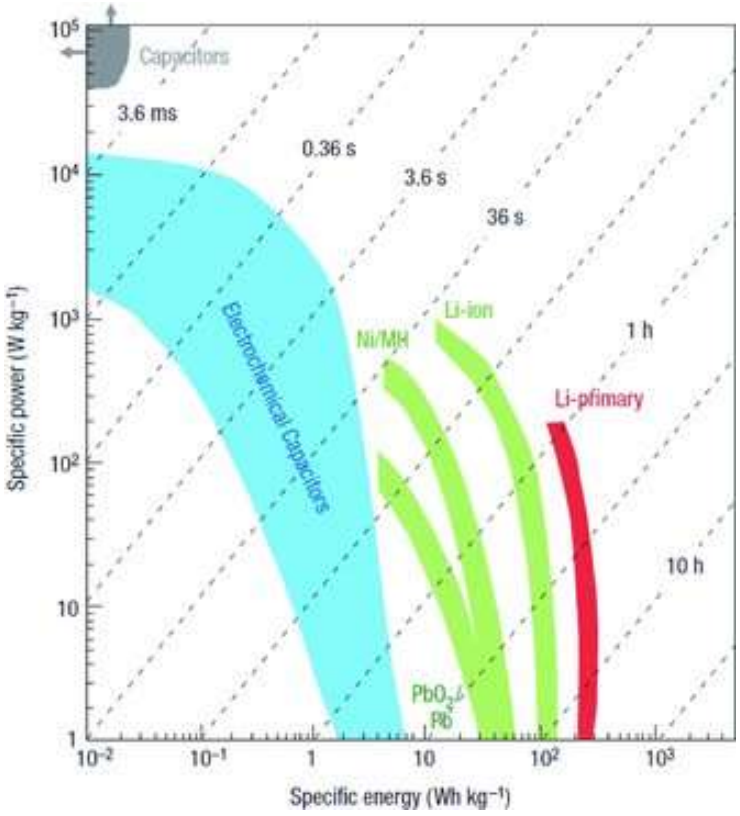

Figure 1.2 Ragone plot showing the specific power against specific energy for various electrical energy storage systems (Reprinted with permission, Ref 16 copyright (2008), Rights Managed by Nature Publishing Group)

1.2.2 Lithium-ion battery

The charge storage mechanism for LIB is different from ECs; Li ions are intercalated into the active material during the charge/discharge process. The configuration of LIB is shown in **Figure 1.3**, where the cathode and anode are made of different materials. [10]

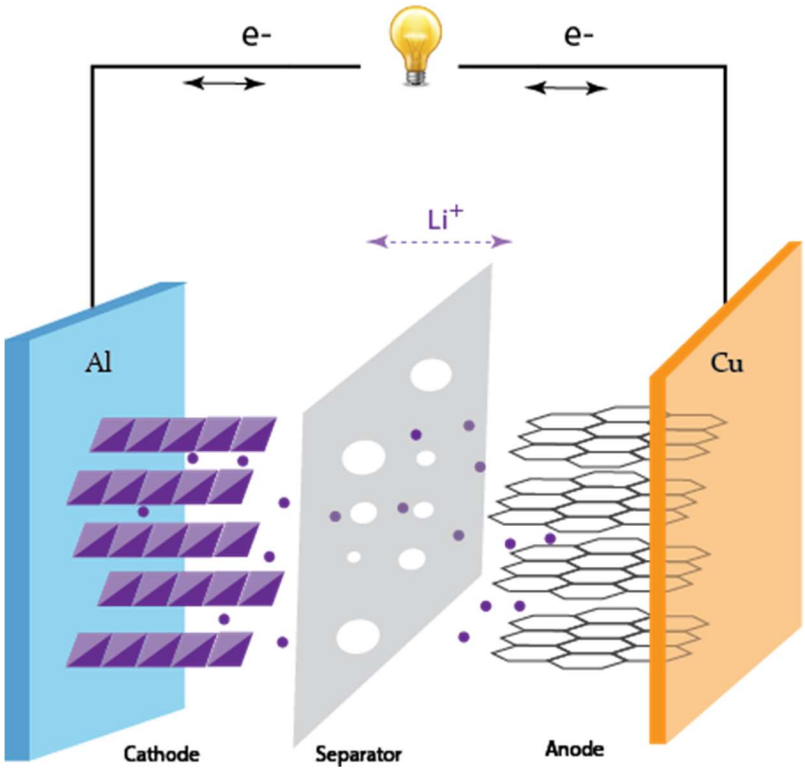

Figure 1.3 Schematic of Lithium-ion Battery

The cathode and anode are classified based on the reduction potential towards Lithium. Cathodes typically have a specific capacity of 150-300 mAh/g with a relatively high voltage range, 3.0-5.0 V vs. Li/Li^+. Lithium transition metal oxides such as $LiCoO_2$, $LiMnO_2$ and phosphate materials such as $LiFePO_4$ are the most commonly used materials

for LIB cathode.[17, 18] During the charge process, the Li ions are intercalated into the cathode and form Lithium transition metal oxide.

Anode has lower intercalation potential (0.1 V vs. Li/Li^+). During the discharge process, the Li ions are deintercalated from the cathode and intercalated into the anode. Carbonaceous materials such as graphite are the most commonly used anode materials for LIB due to its low cost. For the graphite anode, the Li ions intercalate between the graphene layers and form the fully lithiated graphite, LiC_6, which contributing a theoretical capacity of 372 mAh/g with a voltage window of 0.1- 3.0 V.[10] To achieve higher capacity, Si has been investigated since 2008, which has a theoretical capacity of 4200 mAh/g.[19]

1.2.3 Hybrid Supercapacitors

Over the past decades, a large amount of efforts has been devoted to bridging the gap between the high-power density ECs and the high energy density LIB.[20, 21] To enhance the energy density of ECs, the working voltage window needs to be increased. This can be achieved by replacing the aqueous electrolyte by non-aqueous electrolyte or ionic liquids.[20, 22] For the LIB, the power density could be increased by optimizing the particle size and the structure of the electrode.[23, 24]

Hybrid Supercapacitor (HS), so-called supercapacitor-battery hybrid system, is one of the potential solutions to the future energy storage device that produce both high energy density and high-power density. The configuration of the HS is shown in **Figure 1.4**, where one electrode for the device is a capacitive electrode and the other electrode is a battery

one electrode for the device is a capacitive electrode and the other electrode is a battery-type electrode.[25]

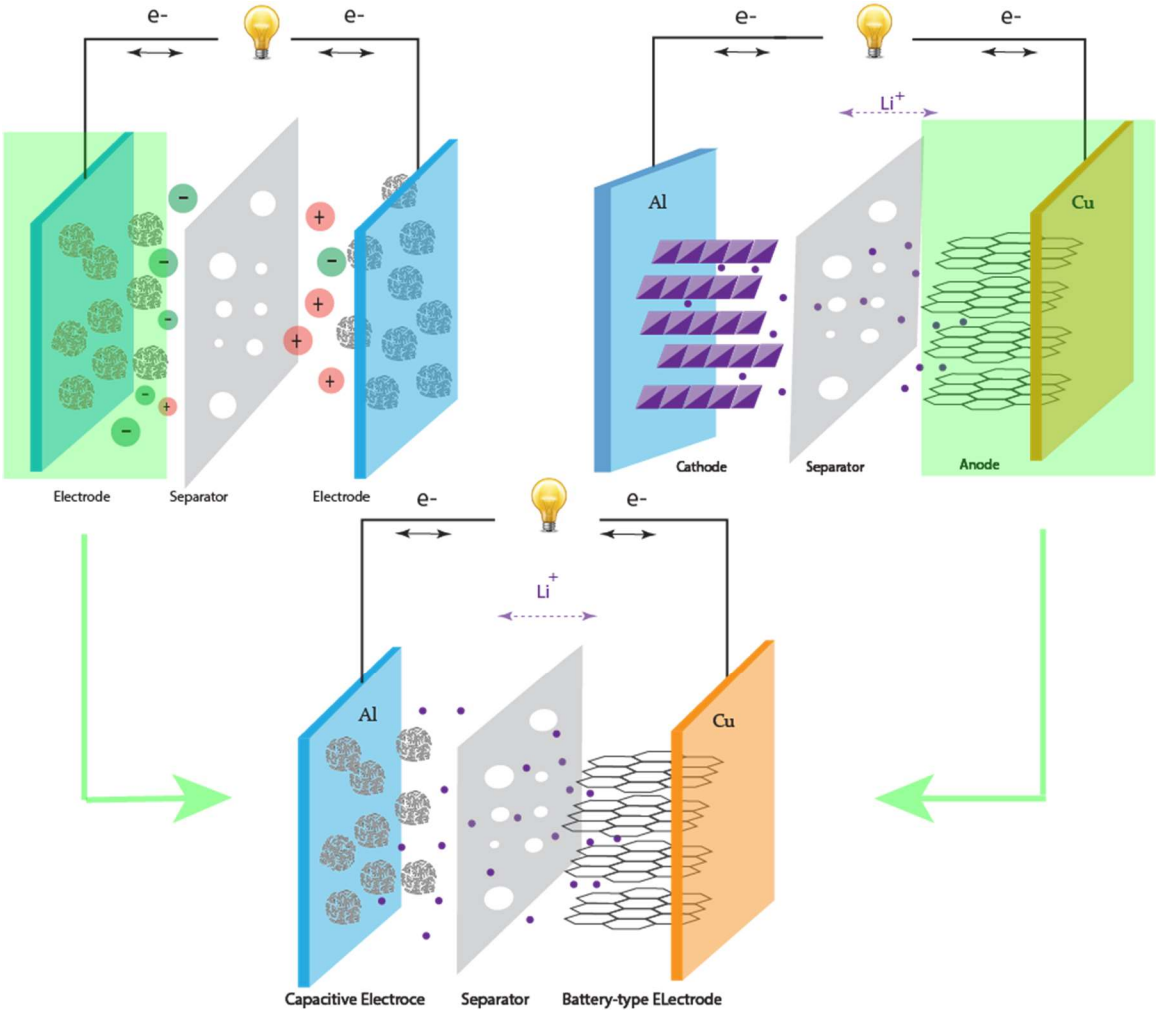

Figure 1.4 Schematic of Hybrid Supercapacitor (Li-ion Supercapacitor)

By replacing one electrode of the symmetric EC with a proper battery-type electrode that works in a higher potential range, the working voltage range of the cell is expanded compared with the symmetric cell.[26] The Hybrid Supercapacitors also have a significantly higher capacitance due to the large capacity of the battery-type electrode. The

most investigated capacitive electrode materials include AC, CNT and graphene. These materials are widely used in as the capacitive electrode material due to their high electrical conductivity and high surface area. However, only EDLC is available in these materials, which limits the capacity of the capacitive electrode to less than 80 mAh/g in the voltage range from 3-4.5 V, which limits the energy density of the hybrid supercapacitors.[27] To solve this problem, tremendous efforts have been devoted to developing new capacitive electrode materials. Li *et al* showed nitrogen doped AC has a high specific capacity of 129 mAh/g in the organic electrolyte at 0.4 A/g.[28] Lee et al showed the oxygen functional group functionalized carbon material (CNT and graphene) is redox-active toward the Li at ~3.2 V vs. Li.[29, 30] The functionalized carbon materials can store charges via both electrical double layer capacitance and pseudocapacitance, which shows the potential of being the capacitive electrode (cathode) of the high-performance hybrid supercapacitor. With this method, various electrode materials were developed for the hybrid supercapacitor.[31-33] The intercalation-type carbon anode can be used as the battery-type electrode. Other material like metal oxide-carbon composite or Si-based materials could also be used as the anode for Li-ion hybrid supercapacitor.[34-36] Several electrolytes could be used in the Hybrid Supercapacitors, including aqueous (H_2SO_4, Li_2SO_4 and KOH etc.), non-aqueous (Lithium Hexafluorophosphate ($LiPF_6$)–ethylene carbonate (EC)–ethyl methyl carbonate (EMC)), ionic liquid, and gel electrolyte.[37]

1.3 Renewable Organic Electrode Materials

With the electrification of vehicles, the demands for the rechargeable battery will keep increasing in the future. Transition metal oxides are widely used as the cathode material for commercial rechargeable batteries. However, transition metals such as Ni, Mn or Co are not renewable. Due to the limitation of the natural mineral resources, the sustainable issue of transition metals has been more and more urgent. Although there is the existing technology of recycling the transition metal from used batteries. It is still urgent to find renewable electrode materials for future rechargeable batteries. Scientists have shown the possibility of lithium-organic battery.[38] *Armand and Tarascon* predicted the electrodes of the future lithium-organic battery are obtained from sustainable earth abundant biomass.[39] The life cycle of the Lithium-organic battery is shown in **Figure 1.5**, where the electrode materials can be recycled from used batteries and carbon-based materials are extracted from the biomass as renewable electrode materials for energy storage devices.[39] Lithium Sulfur battery is another popular research topic since Sulfur is one of the most abundant elements in earth's crust. Sulfur offers a theoretical capacity of 1672 mAh/g, which is one order of magnitude higher than the capacity of the existing trans-metal oxide cathode. Another advantage of the lithium Sulfur battery is the low cost of Sulfur as an industrial waste.[40, 41]

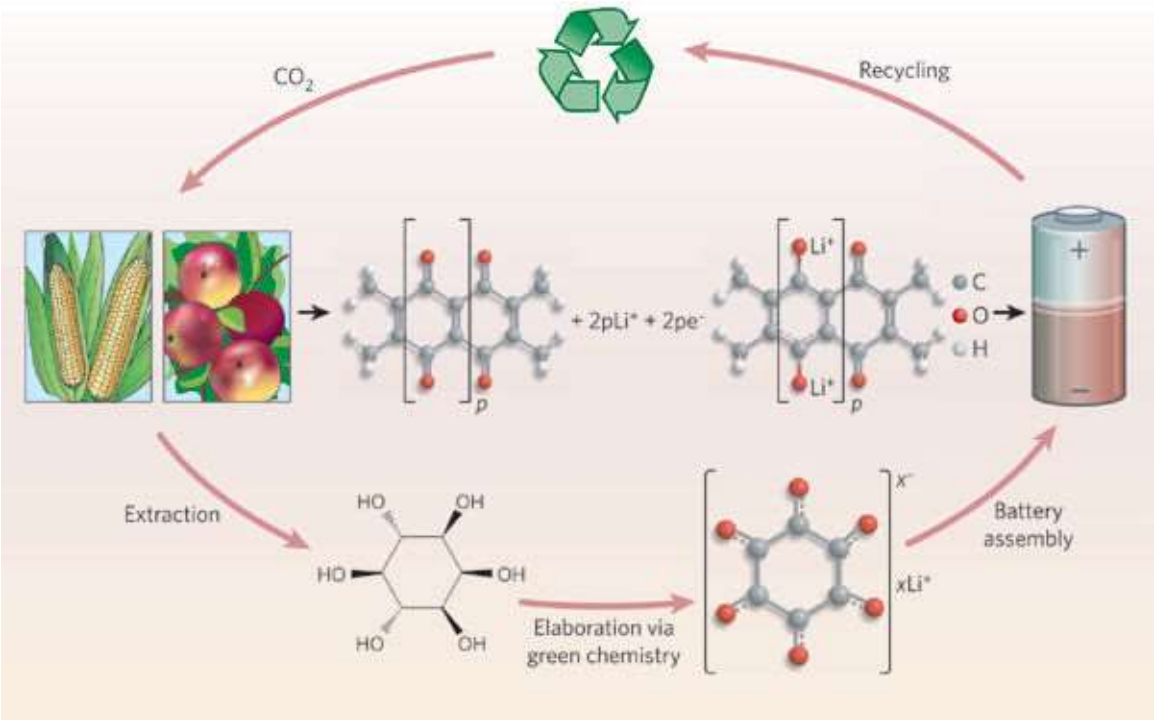

Figure 1.5 An organic future. Proposed sustainable organic-based batteries based on electrode materials made from biomass. (Represented from Ref 39 copyright (2008), Rights Managed by Nature Publishing Group)

1.4 Chapter Organization

1.4.1 Chapter 2

Tetrahydroxyl-1,4-benzoquinone (THQ) was used as reducing agent and functionalizing agent simultaneously for the functionalized graphene hydrogel synthesis. By controlling the mass ratio between the THQ molecule and the GO suspension, the oxygen to carbon ratio of the electrode can easily be tuned. The electrochemical tests were carried out in both aqueous electrolyte and gel electrolyte. By optimizing the loading of THQ molecules, the functionalized graphene electrode showed high specific capacitance

~409 F/g in 1M H_2SO_4 aqueous electrolyte and ~125 F/g in 1 M Li_2SO_4 aqueous electrolyte. In the H_2SO_4-PVA gel electrolyte, the specific capacitance was found ~315 F/g at 1 A/g. The cycling stability of the electrode increased significantly in the gel electrolyte compared with that in the aqueous electrolyte.

1.4.2 Chapter 3

Three quinone group molecules, p-xyloquinone (XQ), 2,5-Dihydroxy-1,4-benzoquinone (DHQ) and 2,5-Dimethoxy-1,4-benzoquinone (DMQ), were used as the functionalizing agent in the synthesis of graphene electrode via hydrothermal reaction. The electrochemical performance of the electrodes was determined in 1M H_2SO_4 aqueous electrolyte. The DHQ functionalized graphene electrode showed the best performance over the three tested quinone group molecules, exhibiting an excellent specific capacitance ~511 F/g at 1 A/g. This is the synergetic contribution of both the unique 3D microstructure and the integrated oxygen functional groups on the surface of the graphene layer. The DHQ functionalized electrode also showed a great cycling stability, maintained 90% of its initial capacitance after 2000 cycles.

1.4.3 Chapter 4

Summary and future research plan are presented.

CHAPTER 2. SELF-ASSEMBLED, THQ FUNCTIONALIZED GRAPHENE ELECTRODE IN AQUEOUS AND GEL ELECTROLYTE

2.1 Introduction

Electrochemical energy storage devices are critical to the development of electric vehicles and sustainable transportation. Electrochemical Capacitor (EC) also known as the supercapacitor or ultracapacitor, is one of the potential energy source for Electric Vehicles and Hybrid Electric Vehicles due to its high-power density and long cycle life. Popular electrode materials for ECs including Activated Carbon (AC), CNT and graphene have been intensively investigated over the past decades due to their outstanding physicochemical properties including high electrical conductivity, high surface area, high mechanical strength, high chemical stability and the abundance of carbon-based material compared to trans-metals. [4, 5]

Graphene, a one-atom-thick graphite material, has been widely studied as the electrode material for SCs and lithium-ion batteries (LIBs).[42] It attracts significant attention due to its high electrical conductivity, low mass density and high specific surface area.[43, 44] In 2008, *Michael*, et al. showed the process of synthesizing the functionalized graphene from graphite.[45-47] With functionalization of graphene, it allows the SCs to store much more capacitance compared to the conventional Electric Double Layer (EDLCs) because of the surface redox storage mechanism, also known as the pseudocapacitance.[48] The synthesis of graphene hydrogels has been reported previously

by *Shi et al* in 2010.[49] With precise control of the synthesis condition, one can synthesize functionalized graphene hydrogel. Herein, we report a graphene-based material for supercapacitor electrode that provides a high specific capacitance of 409 F/g with a capacitance retention of ~70% after 5000 cycles in H_2SO_4-PVA gel electrolyte.

2.2 Experimental

2.2.1 Prepare of Graphene Hydrogel (GH)

The Graphene Oxide single layer dispersion (GO) was prepared by oxidation of natural graphite powder according to the modified Hummers' method with a concentration of 7 mg/ml.[50] 1.43 ml of the GO suspension was diluted to 10 mL (1 mg/mL) with DI water in glass vials. 2,5-Tetrahydroxy-1,4-benzoquinone (THQ, 98% purity, Sigma Aldrich) was added to the GO suspension at different mass ratios (1:1, 1:2, 1:4 and 1:10 respectively as labeled in Figure 2.1(a)). To prepare the GH, the GO-THQ mixture was sonicated for 15 mins and then heated to 80 ℃ for 3 hours. **Figure 2.1(b)** shows the graphene hydrogels (GH) after the heat treatment. After heat treatment, the GHs were washed with DI water for several times to remove the excess THQ until the water become completely clear.

2.2.2 Prepare of Supercapacitor electrode

The synthesized THQ functionalized GH was immersed into the aqueous electrolyte overnight after washing with DI-water. Then the hydrogel was pressed at 10 kN for 3 mins to form a self-supported thin film with a thickness ranging from 18 to 35 um. The thin film was further cut into multiple electrodes with a diameter of 0.635 cm and a

dried mass around 0.6 mg. The dry mass was obtained by parallel measurement, where an electrode with the same mass was washed with water for several times to remove the electrolyte, then dried overnight in the vacuum oven. Similar processes were applied to THQ functionalized GHs with the different mass ratio to prepare the electrodes for the supercapacitor. The detailed information including mass, area, mass loading, thickness and density of the electrodes is given in **Table 1**.

Table 1 Dimensions and specifications of the graphene electrode and the THQ functionalized graphene electrodes with different mass ratio.

	Dry mass (mg)	Area (cm^2)	Mass loading (mg/cm^2)	Thickness (mm)	Density (g/cm^3)
Graphene	1.840	0.317	5.810	0.052	1.117
GO-THQ 1:1	0.440	0.317	1.389	0.025	0.556
GO-THQ 1:2	0.600	0.317	1.895	0.033	0.574
GO-THQ 1:4	0.630	0.317	1.989	0.033	0.602
GO-THQ 1:10	0.640	0.317	2.021	0.039	0.518

2.2.3 Prepare of H_2SO_4 gel-electrolyte

The H_2SO_4 gel-electrolyte was prepared to fabricate the flexible solid-state supercapacitor. First, 1 g of Polyvinyl-Alcohol (PVA) was added to 10 ml of 1M H_2SO_4 solution. The mixture was heated at 85 ℃ under stirring until it became transparent, homogenous mixture. Then the mixture was cooled to room temperature.[51] The Lithium Chloride gel-electrolyte was prepared with the similar method, where 1 g of PVA was added to 10 ml DI water. The mixture was heated at 85 ℃ under stirring until it became

transparent, homogenous mixture. Then 0.42 g of LiCl was added to the gel. The LiCl-PVA mixture was again heated at 85 ℃ under stirring to form LiCl gel electrolyte.[52]

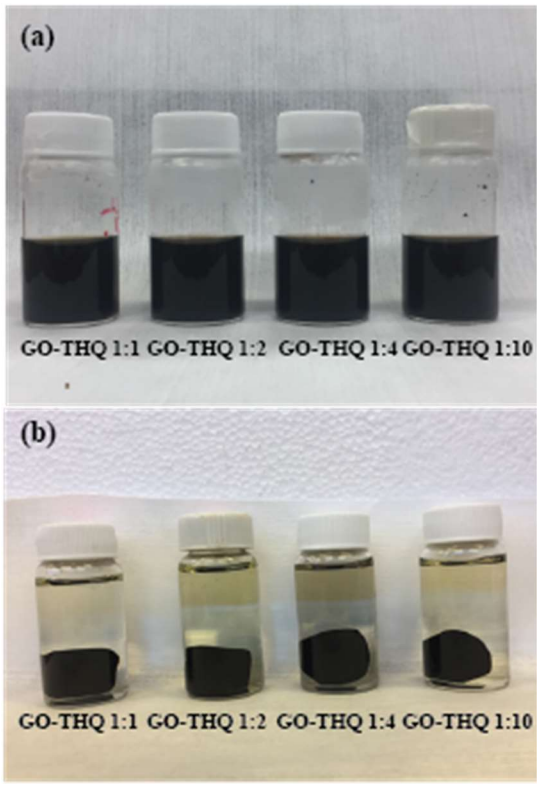

Figure 2.1 (a) GO-THQ mixture at different mass ratio before heat treatment. (b) Graphene hydrogel synthesized after heated for 3 hours.

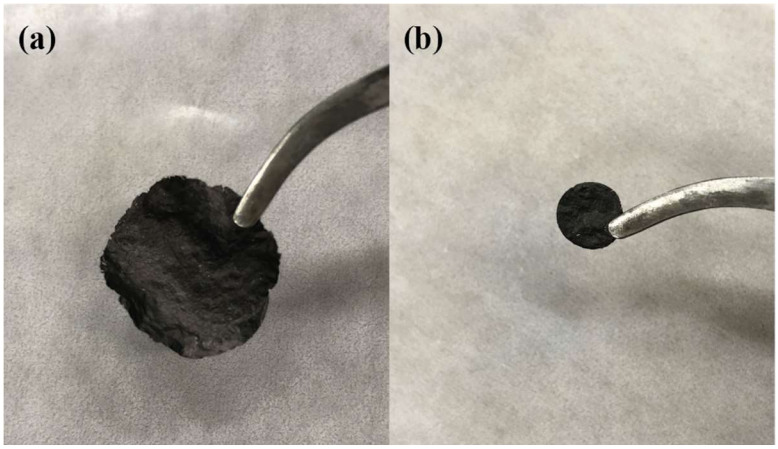

Figure 2.2 (a) Thin film obtained by pressing hydrogel at 10 KN for 3 minutes. (b) Electrode cut from the GH thin film.

2.2.4 Assemble the supercapacitor

The prepared electrode was used to assemble supercapacitor for the electrochemical tests. The supercapacitor used a symmetric configuration (two electrode system), where no reference electrode was used in this experiment. As shown in **Figure 2.3**, two pieces of Platinum foils were used as the current collector of the supercapacitor. The electrode was placed onto the Platinum foil with the two electrodes separated by the Celgard 3510

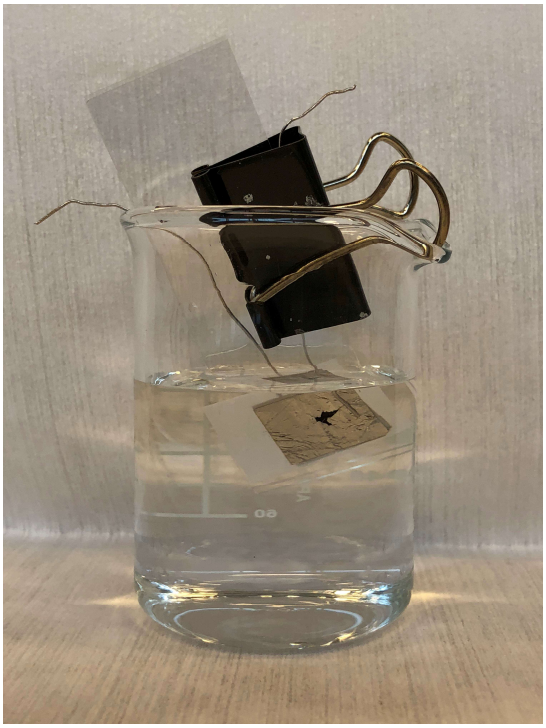

Figure 2.3 Experimental setup for Cyclic Voltammetry (CV), Charge-Discharge test, Electrochemical Impedance Spectroscopy (EIS) and Cycling Stability test.

polypropylene membrane. The two current collectors were pressed together by two glass plates. The assembled cell was immersed into the electrolyte for the Cycle Voltammetry (CV), charge-discharge test and cycling stability test.

2.3 Results and Discussion

2.3.1 Characterization

The redox-active oxygen group on the surface of the graphene electrode can be manipulated by controlling the mass ratio of the GO and THQ. The electrode specifications are listed in **Table 1**, where the GO-THQ 1:10 electrode shows the maximum mass compared to the electrode with other mass ratios. The Scanning Electron Microscope (SEM) images for the rGO electrode and the THQ functionalized graphene electrodes are

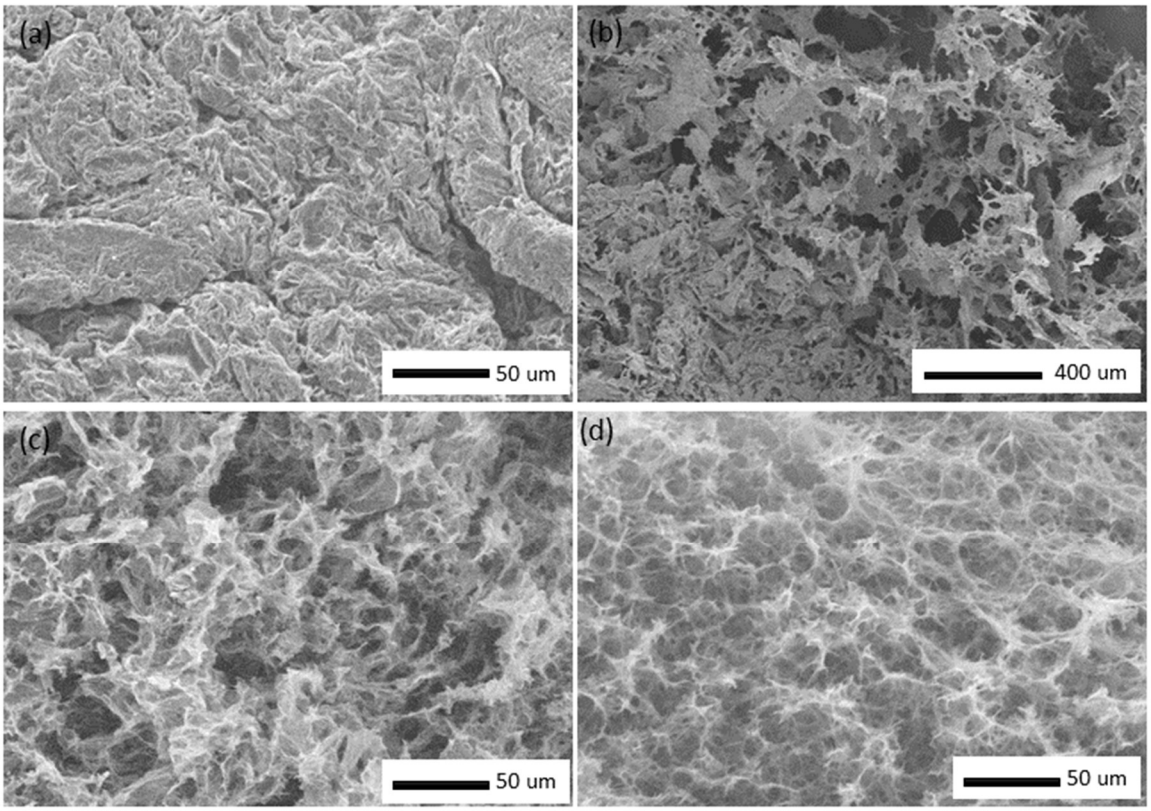

Figure 2.4 Low-magnification Scanning Electron Microscope (SEM) images of the rGO aerogel and THQ functionalized graphene aerogel with different GO-THQ mass ratio. (a) rGO electrode, (b) GO-THQ 1:2, (c) GO-THQ 1:4 and (d) GO-THQ 1:10

shown in **Figure 2.4**, where the synthesized graphene hydrogel was freeze-dried before the SEM. As shown in **Figure 2.4 (a)**, the rGO electrode has a rough surface but not as porous as the THQ functionalized graphene. For the THQ functionalized graphene electrode, it has an interconnected porous 3D structure. As the GO to THQ mass ratio increased, the microstructure became more porous. The GO-THQ 1:10 graphene electrode showed the most porous structure among all the characterized electrodes with the pore size ranging from several micrometers to ~20 micrometers in diameter. The highly porous structure has many advantages in charge storage. (1) The interconnected 3D structure has smaller internal resistance.[53, 54] (2) The pores within the electrode acting as channels for the ion transfer.[55, 56] By providing larger contacting area of the electrode and the electrolyte, it decreases the ion transfer distance, resulting in better performance for high-power applications.

The X-ray Photoelectron Spectroscopy (XPS) scans of the rGO electrode and the THQ functionalized electrodes are shown in **Figure 2.5** and **Figure 2.6**. In **Figure 2.5**, the wide scan survey of the electrodes showed the increase of oxygen/carbon ratio as the THQ concentration increase. The XPS C1s spectra of the electrodes showed the increase of the oxygen functional group (C=O) as THQ concentration increase in the electrodes.

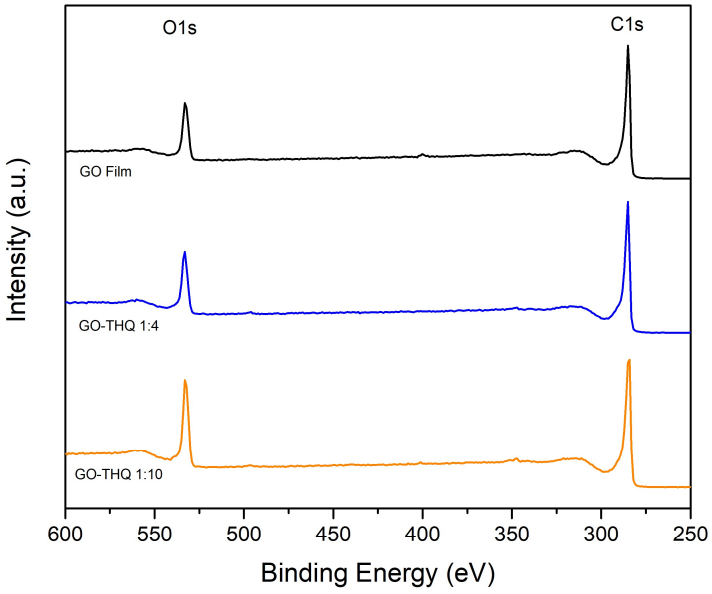

Figure 2.5 XPS wide scan survey of the GO film and THQ functionalized electrodes with different mass ratios (1:4 and 1:10).

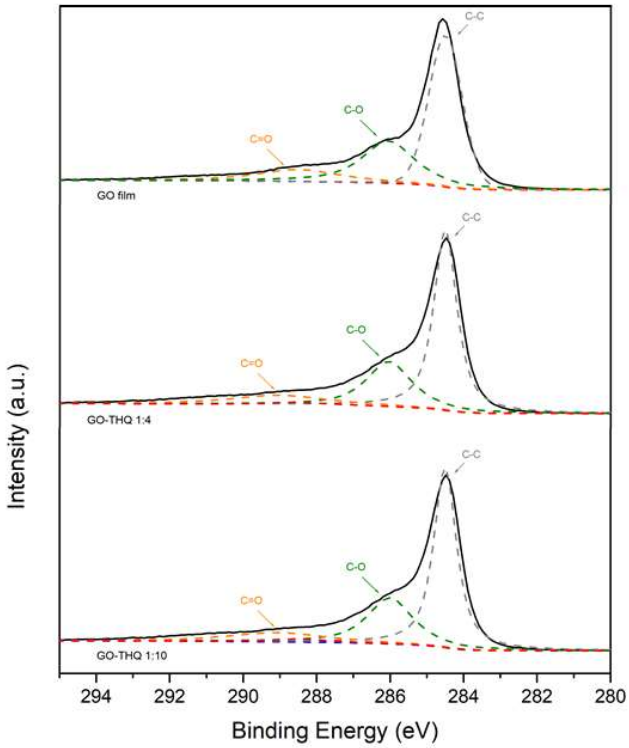

Figure 2.6 XPS C1s spectra of the GO film and THQ functionalized electrodes with different mass ratios (1:4 and 1:10).

2.3.2 Electrochemical tests in 1M H_2SO_4 aqueous electrolyte

Cycling Voltammetry (CV) scan was measured for the THQ functionalized GH electrodes and the RGO electrode. **Figure 2.8** shows the CV curve of rGO electrode and THQ functionalized graphene electrodes from 0-1 V at a scan rate of 5 mV/s, where the CV curve of the rGO electrode exhibits a rectangular shape, which suggests pure EDLC.[57] In contrast, the CV curves for the THQ functionalized graphene electrodes show obvious redox peaks within the voltage range from 0.25 to 0.5 V and from 0.5 V to 0.8 V. The reversible redox peaks imply the existence of pseudocapacitance.[58] The electrodes with the higher concentration of THQ showed larger redox peaks, this means that the pseudocapacitance is due to the functionalization of the THQ. During the heat treatment, H^+ released from the THQ can reduce the oxygen functional groups on the surface of the GO. The reduced Graphene Oxide forms a hydrophobic gel, where the excess THQ and oxide THQ ($C_6O_6H_x$) were absorbed to the surface of the reduced GO by π- π interaction forming the functionalized graphene hydrogel.[59] **Figure 2.7** shows the mechanism of the synthesis process, during which the GO and THQ mixture was heated to 80℃ for 3 hours. The surface Oxygen functional group of the graphene electrodes can be systematically controlled by varying the concentration of THQ in the GO-THQ mixture. Therefore, additional redox-active oxygen functional groups can be incorporated onto the surface of the graphene electrode.

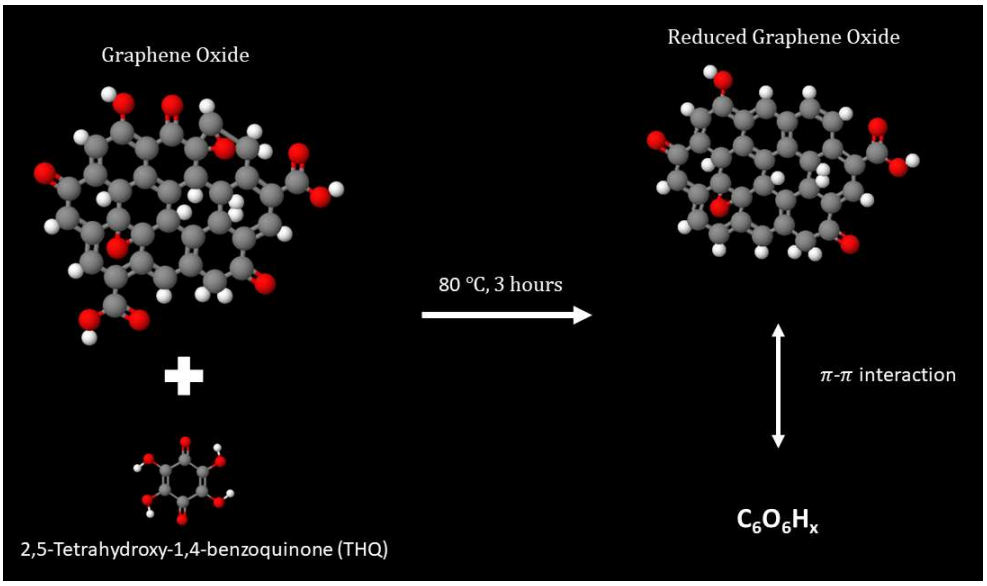

Figure 2.7 The mechanism of the synthesis process of the functionalized graphene. (Reprinted with permission, Ref 59 copyright (2014), Rights Managed by American Chemical Society Publishing Group)

It is clearly shown in **Figure 2.8**, with the increase of the THQ concentration, the faradic peak shows a clear increase in the amplitude. This indicates the faradic peaks are due to the functionalization of the THQ, providing the redox reaction of the carbonyl group (C=O) with the proton in the electrolyte. The electrochemical redox reaction mechanism of THQ in 1M aqueous H_2SO_4 is shown as **Equation 1**.[47, 60]

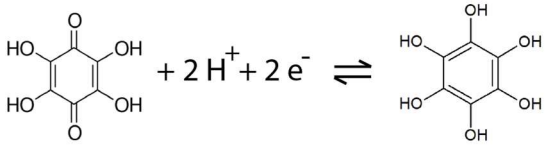

(1)

The specific capacitance of the rGO electrode and THQ functionalized graphene electrodes can be calculated with the following **Equation 2**,[52, 61]

$$C = \frac{\int I \, dV}{\Delta V \cdot V \cdot m} \tag{2}$$

where C is the specific capacitance, I is the current, ΔV is the scan rate, V is the voltage window and m is the mass of the electrode. The specific capacitance of the GO-THQ 1:10 electrode calculated to be 403 F/g based on the CV scan at 5 mV/s, which is significantly higher than the specific capacitance of the rGO electrode (211 F/g). The CV scans for the THQ functionalized electrodes with the different mass ratio at various scan rate are shown in **Figure 2.9**. The CV curves showed rectangular shapes with redox peaks for scan rate from 5 mV/s to 50 mV/s. However, the CV curve distorted to an olive shape at 100 mV/s, which can be attributed to the larger resistance at the higher scan rate.[62]

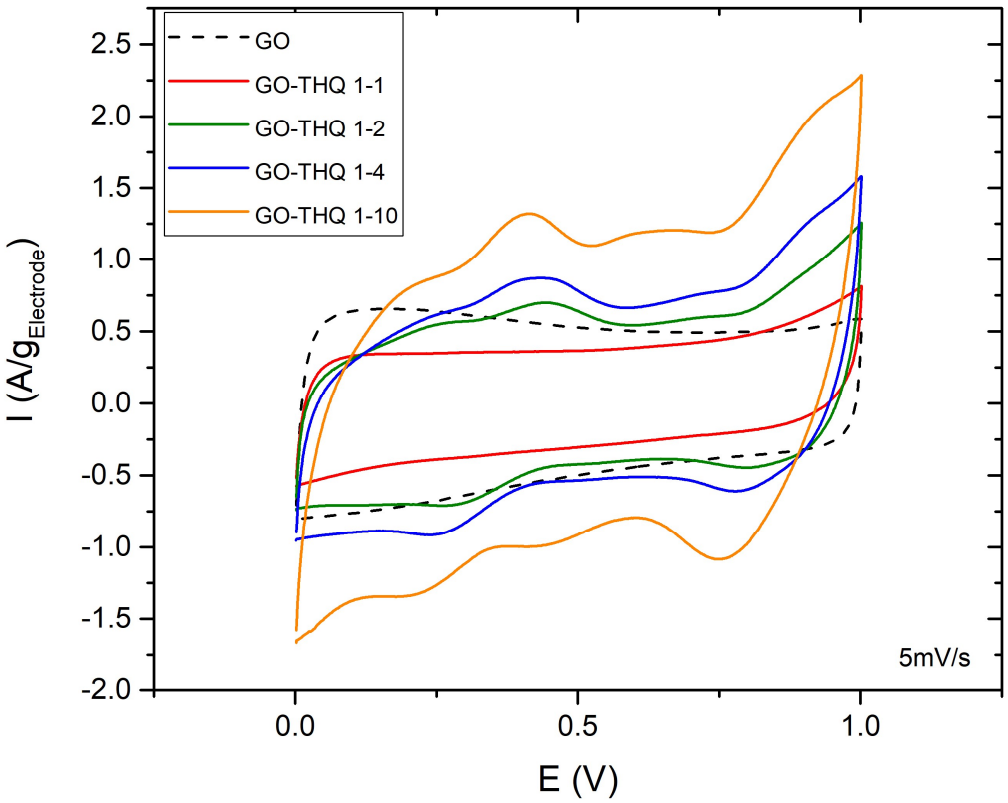

Figure 2.8 Comparison of the steady-state cycling voltammetry (CV) scans of the rGO electrode and THQ functionalized graphene electrodes with different THQ concentration ratios of 1:1, 1:2, 1:4 and 1:10 in 1 M H_2SO_4 electrolyte, the voltage window of the CV was 0-1 V

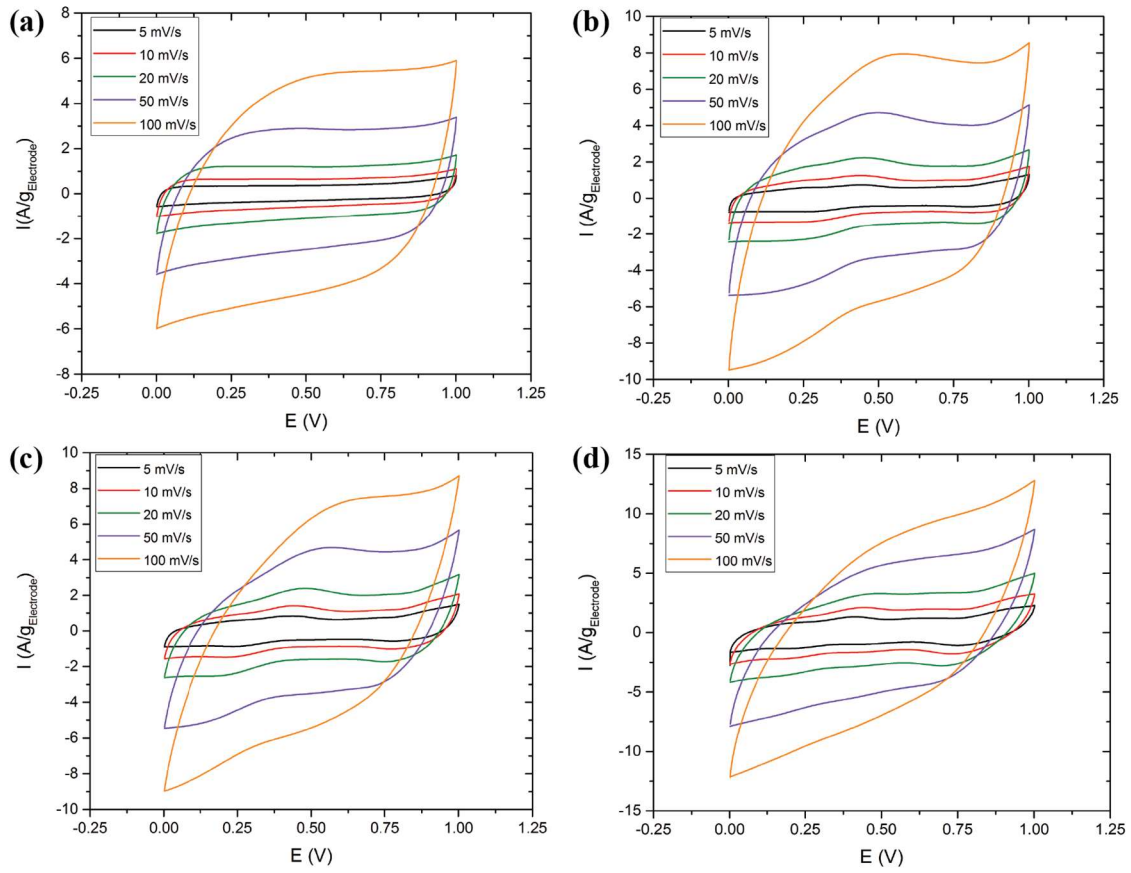

Figure 2.9 CV at scan rates of 5 mV/s, 10 mV/s, 20 mV/s, 50 mV/s and 100 mV/s for THQ functionalized graphene electrodes with different mass ratio. (a) GO-THQ 1:1, (b) GO-THQ 1:2, (c) GO-THQ 1:4 and (d) GO-THQ 1:10.

The galvanostatic charge-discharge test was to measure the galvanostatic specific capacitance of the THQ functionalized graphene electrodes. The charge-discharge curves of the electrodes at the current density of 1 A/g are displayed in **Figure 2.10**. The charge-discharge curve of the rGO electrode shows a rectangular shape, which indicates a pure Electrical Double Layer Capacitance. As the mass ratio of the electrode increase, the charge-discharge curve starting distorting. The charge-discharge curve of GO-THQ 1:10 is clearly distorted, which attributes to the reversible redox reaction. The galvanostatic specific capacitance was estimated based on the charge-discharge curve using **Equation 3**,

$$C = \frac{2 \cdot I \cdot \Delta t}{V} \tag{3}$$

where I is the current density in A/g, V is the voltage window of the charge-discharge test, Δt is the discharge time in seconds.[52] The specific capacitance of the GO-THQ 1:10 electrode was estimated to be 409.64 F/g, 345.38 F/g, 250.74 F/g, 163.24 F/g and 67.29 F/g at 1 A/g, 2 A/g, 5 A/g, 10 A/g and 20 A/g. The galvanostatic specific capacitance of the rGO electrode and THQ functionalized graphene electrodes with the different mass ratio at 1-20 A/g are displayed in **Figure 2.11**., where only the GO-THQ 1:4 electrode and the GO-THQ 1:10 electrode showed higher specific capacitance compared with rGO electrode at all current densities. Thus, the cycling stability was only tested for the GO-THQ 1:4 electrode and the GO-THQ 1:10 electrode at a current density of 5 A/g for 5000 cycles using the experimental setup in **Figure 2.3.** The cycling stability results are shown in **Figure 2.12.**

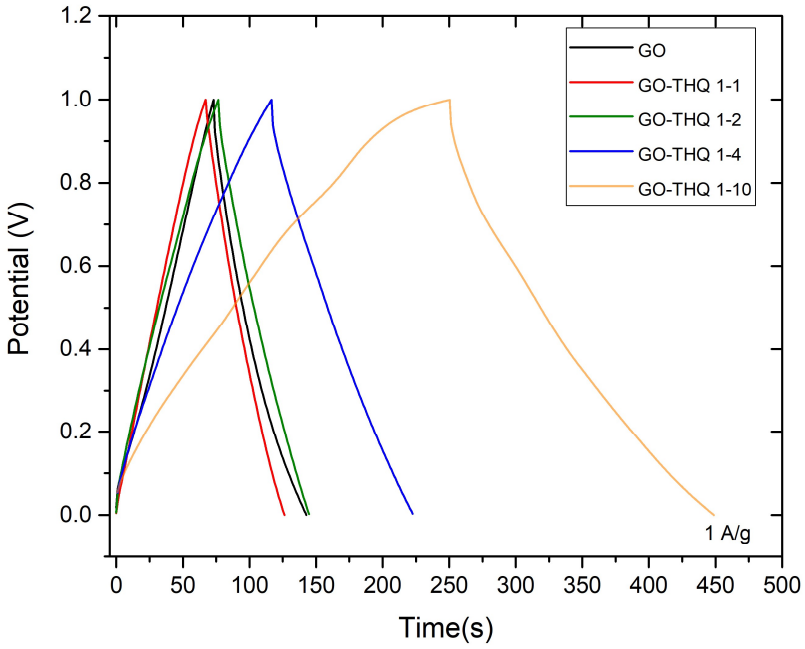

Figure 2.10 Galvanostatic charge-discharge curves of rGO electrode and THQ functionalized graphene electrodes with mass ratio of 1:1, 1:2, 1:4 and 1:10 in 1M H_2SO_4 electrolyte at current density of 1 A/g.

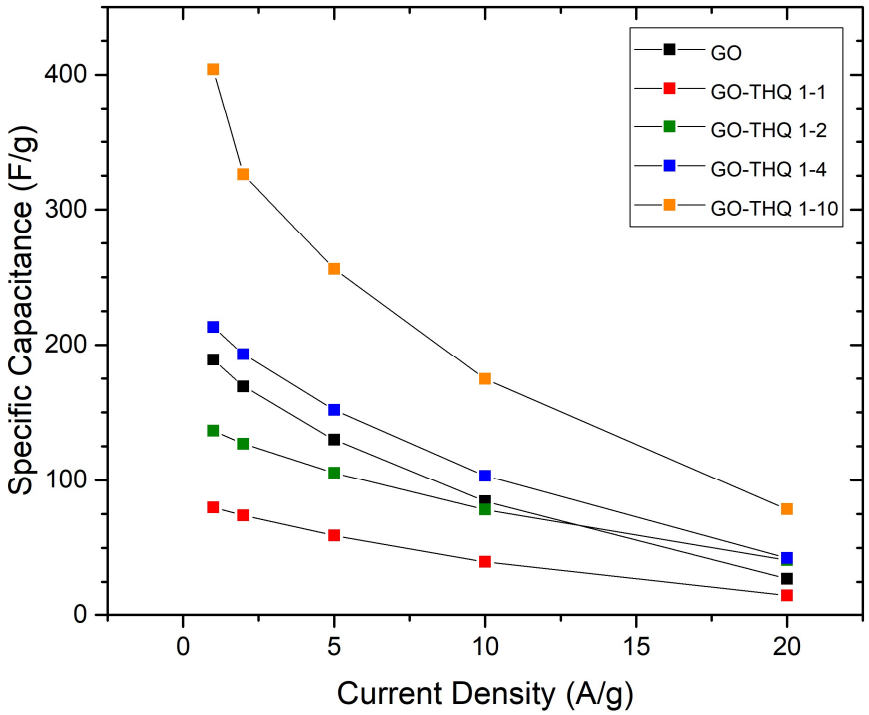

Figure 2.12 Galvanostatic specific capacitance of rGO electrode and GO-THQ electrodes with different mass ratio at 1, 2, 5, 10 and 20 A/g

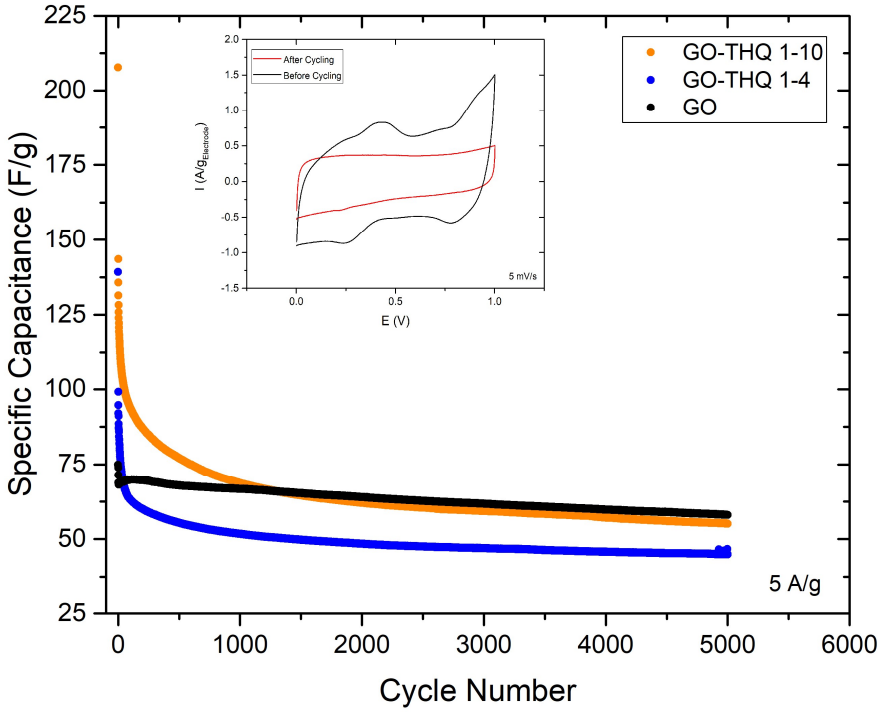

Figure 2.11 Cycling stability test of rGO electrode, GO-THQ 1:4 and 1:10 electrode in 1 M H2SO4 aqueous electrolyte at 5 A/g. Inserted the comparison of CV scans for GO-THQ 1:4 electrode before and after 5000 cycles of cycling stability test at scan rate of 5 mV/s.

The specific capacitance of the THQ functionalized graphene electrode decayed significantly (from 209 F/g to ~75 F/g) during the first 500 cycles. After 2000 cycles, the specific capacitance stabilized at ~65 F/g for the GO-THQ 1:10 electrode and ~50 F/g for the GO-THQ 1:4 electrode. The specific capacitance retention for the GO-THQ 1:10 electrode is around 31%. The inserted figure showing the CV scan of the GO-THQ 1:4 electrode at 5 mV/s before and after the cycling stability test. The redox peaks are obvious on the CV scan for the GO-THQ 1:4 electrode before the cycling stability test. However, the CV scan of the electrode after 5000 cycles in the 1M H_2SO_4 aqueous electrolyte only showed a rectangular shape, which indicates a pure EDLC charge storage. The dissolution the THQ molecules that functionalize the graphene is the main reason for the decay of the specific capacitance during the cycling test.[63] **Figure 2.13** showed two CV scans of the same GO-THQ electrode at 5 mV/s with a time gap between two months. The CV scans also confirmed that the solvation of the function group is the main reason for the decay of the specific capacitance. The conductivity and ion transport of the THQ functionalized graphene electrode with different mass ratio was tested via Electrochemical Impedance Spectroscopy (EIS), the Nyquist plot is shown in **Figure 2.14**. The semicircle area on the Nyquist plot indicates the interfacial charge transfer resistance increases as the more THQ are loaded onto the surface of the graphene. The electrode higher GO-THQ mass ratio showed stronger deviation from the vertical line, implying a higher Warburg resistance, which is caused by the pseudocapacitance of the THQ molecules integrated to the graphene surface.[64]

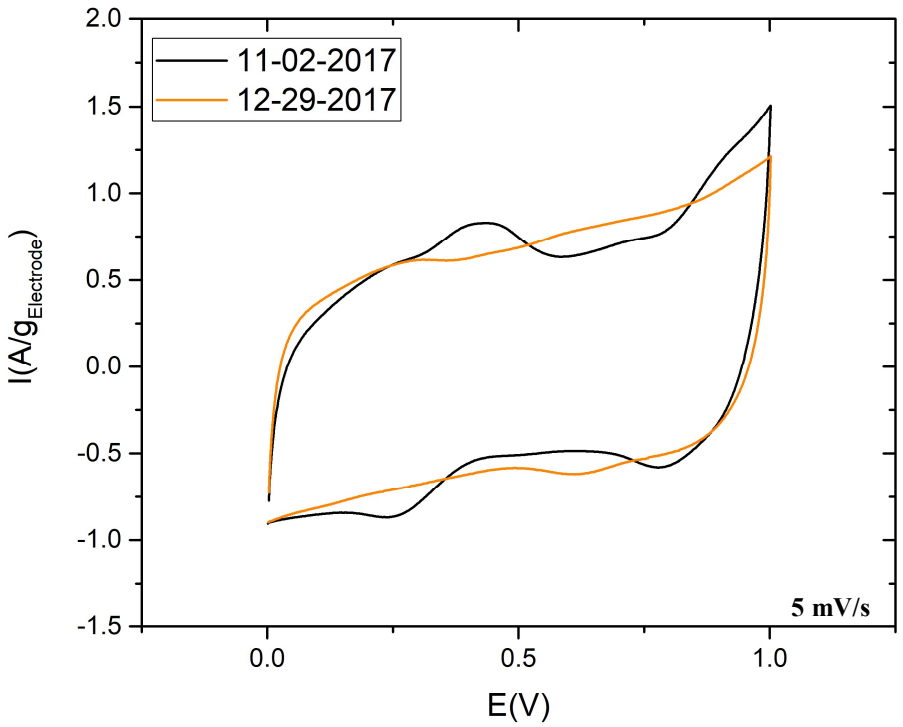

Figure 2.14 Steady-state CV scans of the same GO-THQ 1:10 electrode at 5 mV/s on two different dates with time difference of 2 months.

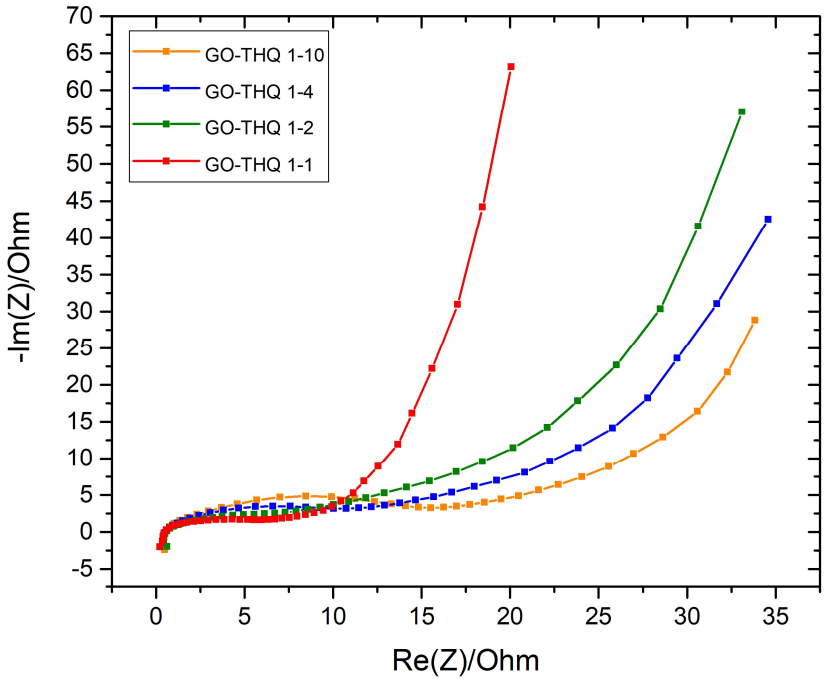

Figure 2.13 Electrochemical Impedance Spectra of THQ functionalized graphene electrode with different mass ratio.

2.3.3 Electrochemical Tests in Li_2SO_4

The electrochemical tests were also conducted in 1M Li_2SO_4 aqueous electrolyte for the GO functionalized graphene electrodes. The CV scans with two different voltage windows (0-1 V and 0-1.6 V) were carried out for the THQ functionalized graphene electrodes with different mass ratios. The CV curves from 0 to 1 V for the THQ functionalized graphene electrodes at different scan rates are shown in **Figure 2.15**.

The CV scans of electrodes with the different mass ratio over various voltage windows are displayed in **Figure 2.16**. Reversible redox peak can be observed from 0.2 to 0.5 V and 0.75-1.2 V. **Figure 2.17** is the comparison of THQ functionalized graphene electrodes with different mass ratio at scan rate of 5 mV/s from 0 to 1.6 V. By using the 1M Li_2SO_4 aqueous electrolyte, a larger voltage window can be used for the electrochemical supercapacitor, which increases the energy density of the cell. In **Figure 2.16**, the THQ functionalized electrodes showed larger redox peak as the mass ratio of the GO to THQ increase from 1:1 to 1:10.

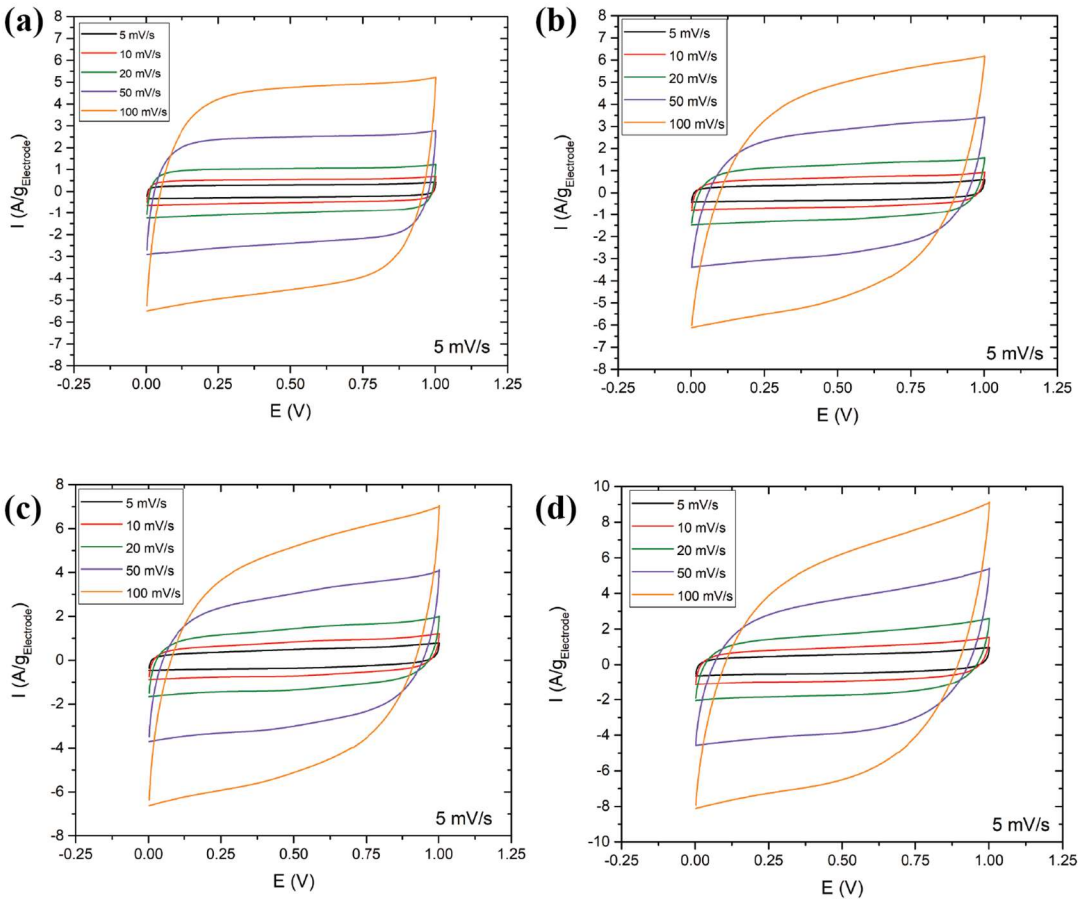

Figure 2.15 Steady-state CV scans at different scan rates, 5, 10, 20, 50 and 100 mV/s for THQ functionalized graphene electrodes with different mass ratio in 1 M Li_2SO_4 electrolyte from 0 to 1 V. (a) GO-THQ 1:1, (b) GO-THQ 1:2, (c) GO-THQ 1:4 and (d) GO-THQ 1:10.

Like the CV scan in 1M H_2SO_4 aqueous electrolyte, the GO-THQ 1:1 electrode did not show redox peak in the 1M Li_2SO_4 aqueous electrolyte, the rectangular shape of the CV scan indicates the GO-THQ 1:1 electrode has purely EDLC charge storage. Redox peak can be observed from 0.3 to 0.8 V for the GO-THQ 1:4 electrode. The specific capacitance was estimated using Equation 2, which gives a specific capacitance of 195.05 F/g for the THQ functionalized graphene electrode at the mass ratio of 1:10.

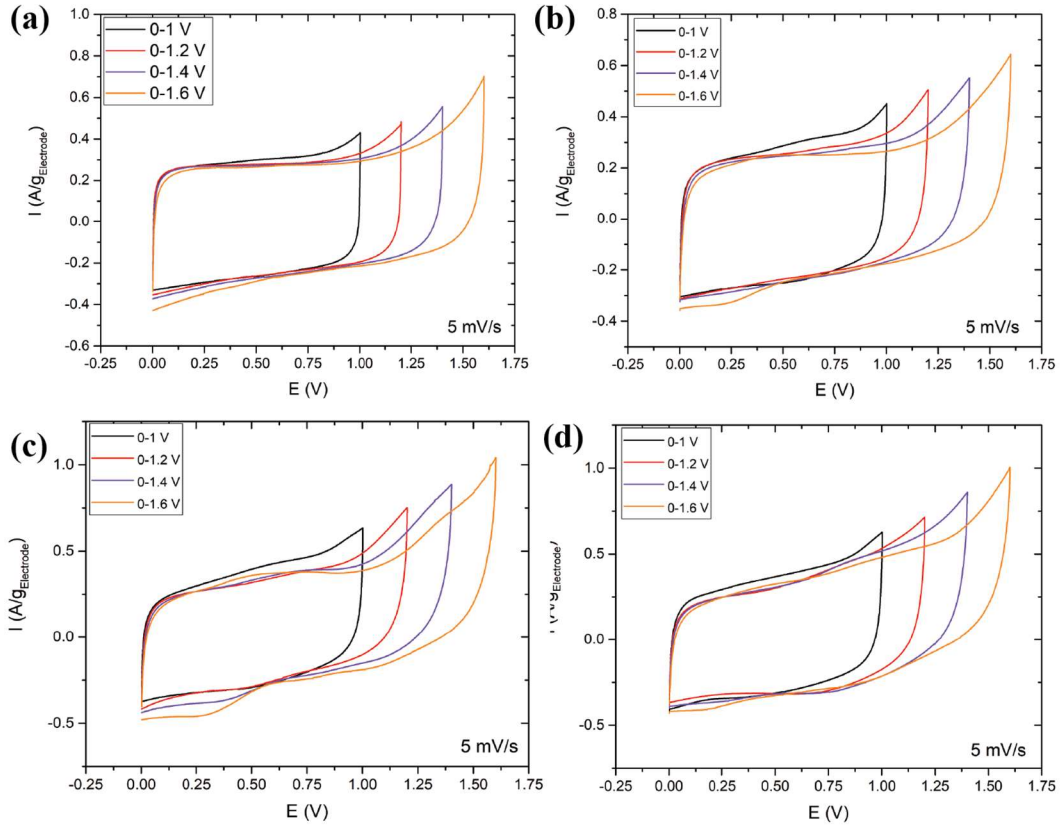

Figure 2.16 Steady-state CV scans at 5 mV/s scan rate for THQ functionalized graphene electrodes with different mass ratio in 1 M Li_2SO_4 aqueous electrolyte using various voltage windows. (a) GO-THQ 1:1, (b) GO-THQ 1:2, (c) GO-THQ 1:4 and (d) GO-THQ 1:10.

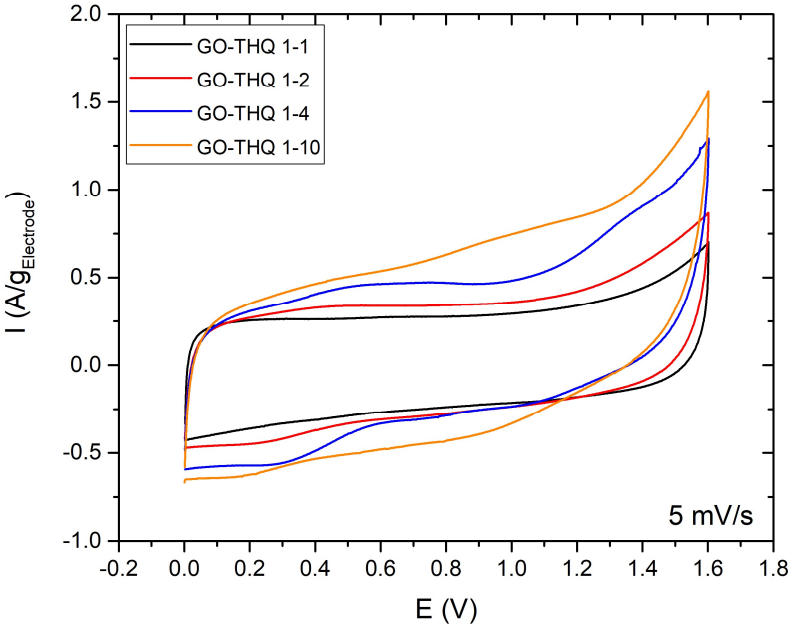

Figure 2.17 Comparison of the steady-state CV scans of the THQ functionalized graphene electrodes with different mass ratio of 1:1, 1:2, 1:4 and 1:10 in 1 M Li_2SO_4 electrolyte, the voltage window of the CV was 0-1.6 V at scan rate 5 mV/s.

The galvanostatic charge-discharge curves for the electrodes are showing in **Figure 2.18.** At 1 A/g current density, the GO-THQ 1:10 electrode showed a distorted charge-discharge curve, which is consistent with the result of the CV scan. This confirms the

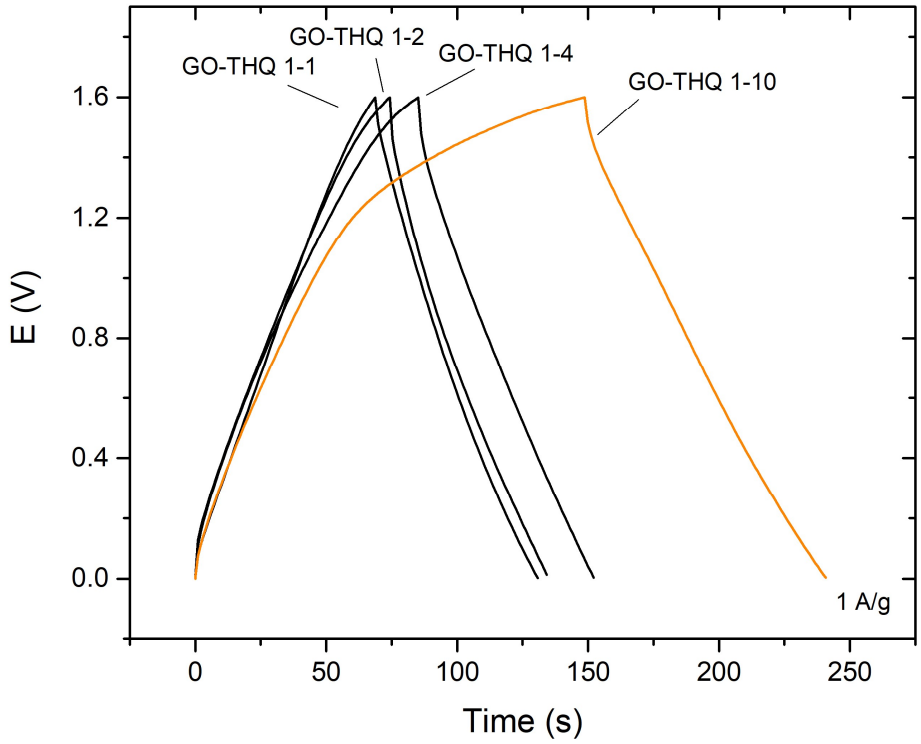

Figure 2.18 Galvanostatic charge-discharge curves of THQ functionalized graphene electrodes with mass ratio of 1:1, 1:2, 1:4 and 1:10 in 1 M Li_2SO_4 electrolyte at current density of 1 A/g.

redox-reaction between the functional molecule (THQ) and the Li^+ ions since the redox peak increases as the concentration of THQ increases in the GO-THQ mixture.

The galvanostatic specific capacitance was calculated with **Equation 3** for the electrodes at different current densities. The current density dependent specific capacitance is shown in **Figure 2.19**. At 1 A/g, the GO-THQ 1:10 functionalized graphene electrode has a specific capacitance ~125 F/g. At a higher current density of 5 A/g, the GO-THQ 1:10 electrode still showed a specific capacitance over 100 F/g, which is higher than other

electrodes with lower THQ concentrations. The cycling stability test was conducted at 1 A/g in 1M Li_2SO_4 aqueous electrolyte for the electrode with the best electrochemical performance, which is the GO-THQ 1:10 electrode. as shown in **Figure 2.20**.

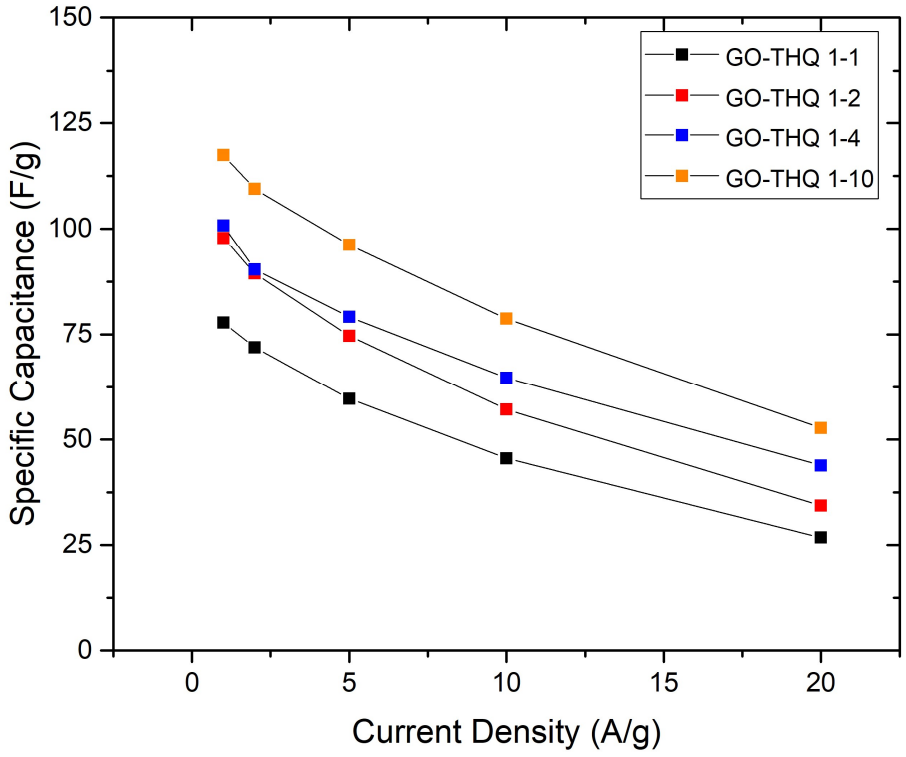

Figure 2.19 Galvanostatic specific capacitance of GO-THQ electrodes with different mass ratio at current density of 1, 2, 5, 10 and 20 A/g.

Like the cycling stability result in the 1M H_2SO_4, the specific capacitance of the THQ functionalized graphene electrode decreased significantly within the first 100 cycles. And the specific capacitance stabilized after 200 cycles at ~75 F/g. Compared with the specific capacitance of the 1st cycle of the cycling stability test, the capacitance retention is around 35%. As previously discussed, this is due to the dissolution of the THQ molecule into the aqueous electrolyte. The inserted comparison between CV scans before and after

the cycling stability test at 5 mV/s shows the disappearance of the redox peak during the cycling stability test.

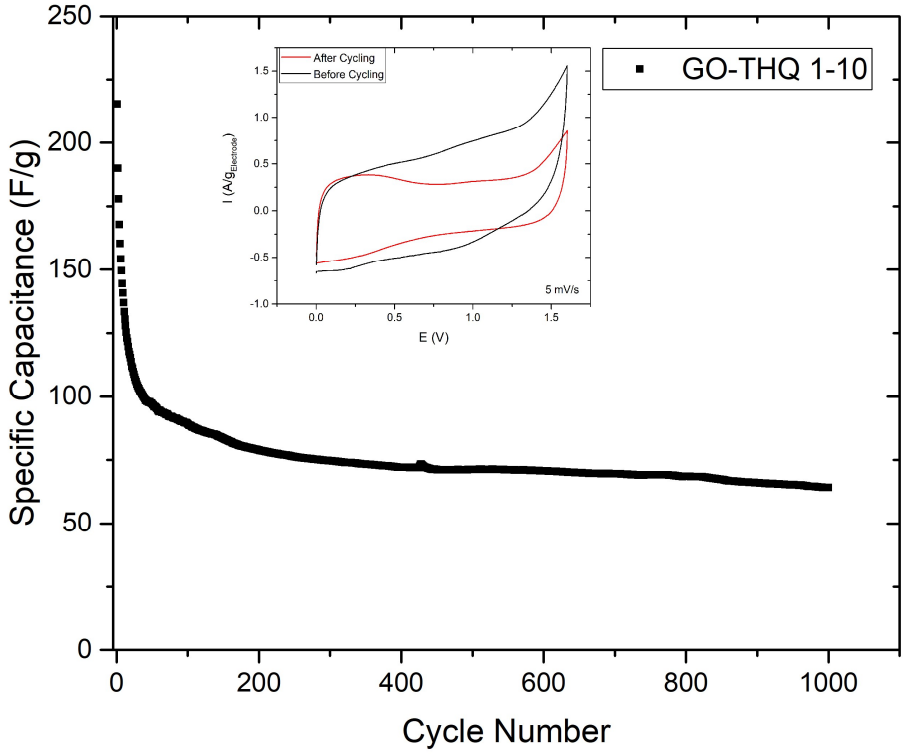

Figure 2.20 Cycling stability test of GO-THQ 1:10 electrode in 1 M Li_2SO_4 aqueous electrolyte at 1 A/g for 1000 cycles. Inserted the comparison of CV scans for GO-THQ 1:10 electrode before and after 1000 cycles of cycling stability test at scan rate of 5 mV/s.

The dissolution of the quinone group molecules into the aqueous electrolyte is a common problem. This is due to the high solubility of THQ in water at room temperature (11g/L at 18 ℃).[65] The SEM images shown in **Figure 2.4** demonstrates the porous structure of the electrode, where the THQ functionalized graphene electrodes showed larger pore size and more porous structure. The pores provide the access for the electrolytes to the active molecules that attached on the surface of the reduced GO via π- π interaction, which improves the performance of the THQ functionalized electrodes. However, the pores

also increased the dissolution rate of the THQ molecules into the aqueous electrolytes, which is the main reason that caused the significant capacitance decrease in the first 200 cycles of the cycling stability test. One potential solution to the poor cycling stability of the THQ functionalized graphene electrode is to use gel electrolyte. In the next section of this chapter, the THQ functionalized graphene electrodes were tested in H_2SO_4-PVA gel electrolyte and the results were compared with the results in the aqueous electrolyte.

2.3.4 Electrochemical Tests in H_2SO_4/PVA Gel Electrolyte

The performance of the THQ functionalized graphene electrodes was tested and compared with the rGO electrode in the H_2SO_4-PVA electrolyte.

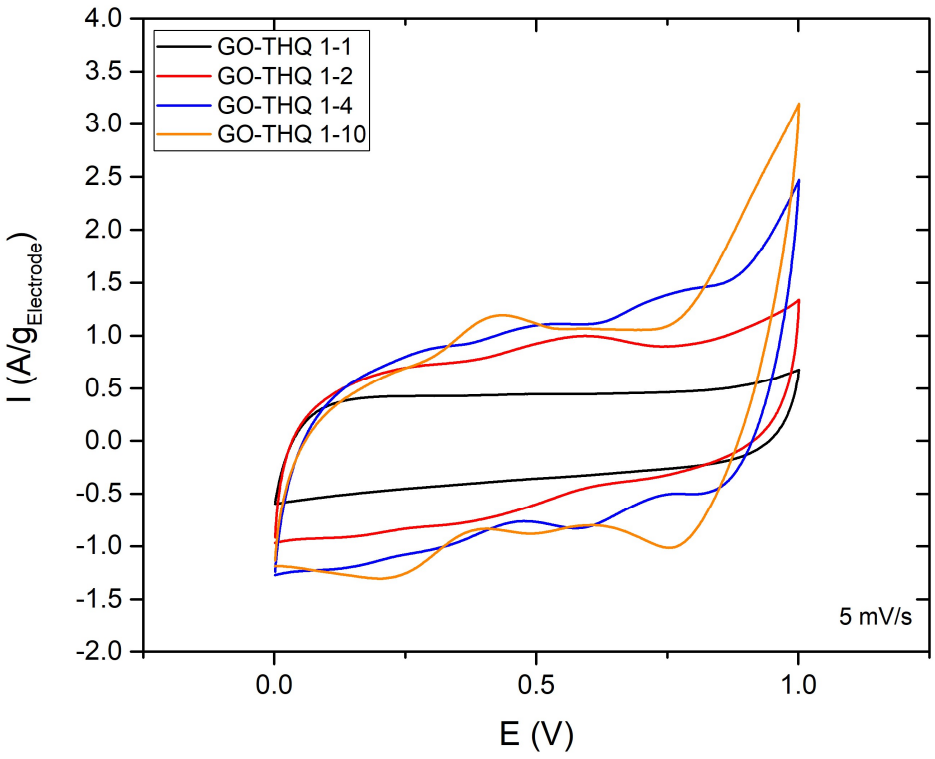

Figure 2.21 Comparison of the steady-state CV scans of the THQ functionalized graphene electrodes with different mass ratio of 1:1, 1:2, 1:4 and 1:10 in H_2SO_4-PVA gel electrolyte, the voltage window of the CV was 0-1 V at scan rate 5 mV/s.

The steady-state CV scans of the rGO electrode and the THQ functionalized electrodes in H_2SO_4-PVA electrolyte are shown in **Figure 2.21**. The GO-THQ electrode showed an ideal rectangular shape indicating pure EDLC charge storage. As the GO-THQ ratio increase from 1:1 to 1:2, redox peak starts showing. With the GO-THQ ratio further increasing, clear redox can be found in 0.25 - 0.5 V and 0.5 - 0.75 Von the CV curve. The specific capacitance of the GO-THQ 1:10 electrode was estimated to be ~360.56 F/g at 5 mV/s. The specific capacitance of the rGO electrode was estimated to be ~70 F/g at 5 mV/s. The improvement in the specific capacitance is credited to the carbonyl functional group attached to the surface of the electrode as well as the porous structure. However, the specific capacitance is smaller compared with the specific capacitance of GO-THQ 1:10 electrode in aqueous H_2SO_4 electrolyte (403 F/g). The reason is the ion diffusivity and the internal resistance of the solid-state cell was larger than the aqueous system. The galvanostatic charge-discharge test was conducted at different current densities for both the rGO electrode and the THQ functionalized graphene electrodes to calculate the current density dependent specific capacitance. **Figure 2.22** shows the galvanostatic charge-discharge curves at 1 A/g for both rGO electrode and the THQ functionalized graphene electrodes. The rGO electrode showed an ideal triangular shape while the THQ functionalized graphene electrodes showed distorted charge-discharge curves due to pseudocapacitance. The current density dependent specific capacitance of all tested electrode was calculated with Equation 3 and shown in **Figure 2.23**. The GO-THQ 1:10 electrode showed specific capacitance of ~314.39 F/g at 1 A/g, ~264.72 F/g at 2 A/g, ~176.50 F/g at 5 A/g and ~90.06 F/g at 10 A/g, which is higher than other electrodes at all current densities.

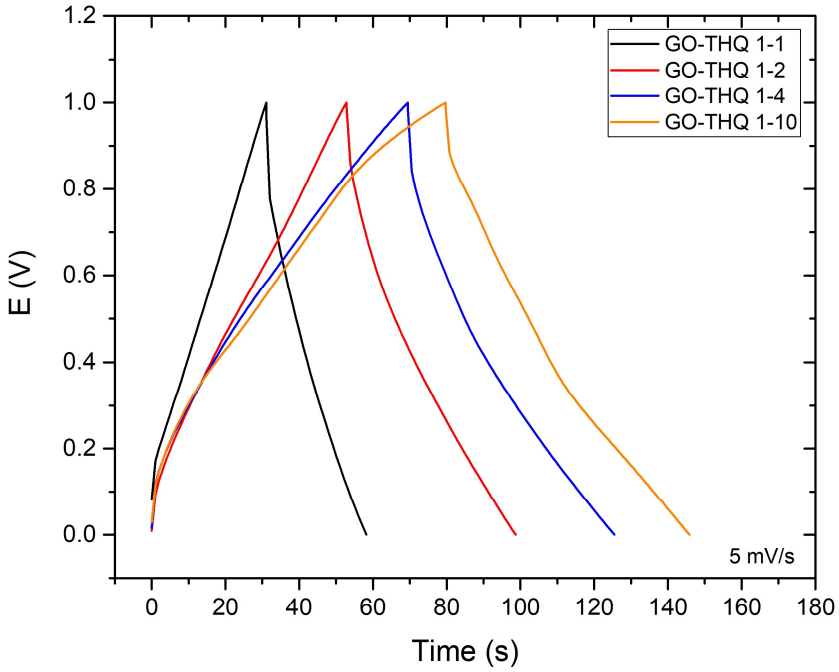

Figure 2.22 Galvanostatic charge-discharge curves of rGO electrode and THQ functionalized graphene electrodes with mass ratio of 1:1, 1:2, 1:4 and 1:10 in H_2SO_4-PVA gel electrolyte at current density of 1 A/g.

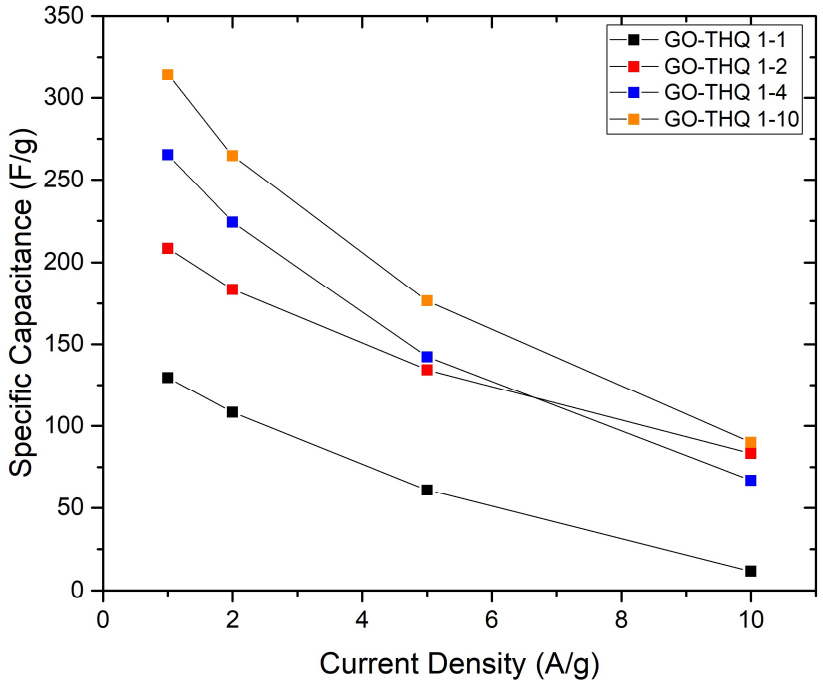

Figure 2.23 Galvanostatic specific capacitance of rGO electrode and GO-THQ electrodes with different mass ratio at current density of 1, 2, 5 and 10 A/g.

The cycling stability of the GO-THQ 1:10 electrode is significantly improved in the H_2SO_4-PVA gel electrolyte. At the first cycle, the electrode showed a specific capacitance of 174.40 F/g, which is closed to the result of the charge-discharge test (176.50 F/g). After 2000 cycles, the specific capacitance of the GO-THQ 1:10 electrode stabilized at 122 F/g, giving a capacitance retention of 70%, which is significantly higher than the 35% capacitance retention in the aqueous electrolyte. **Figure 2.24(a)** is the cycling stability of the GO-THQ 1:10 electrode in the H_2SO_4-PVA gel electrolyte. **Figure 2.24(b)** shows the

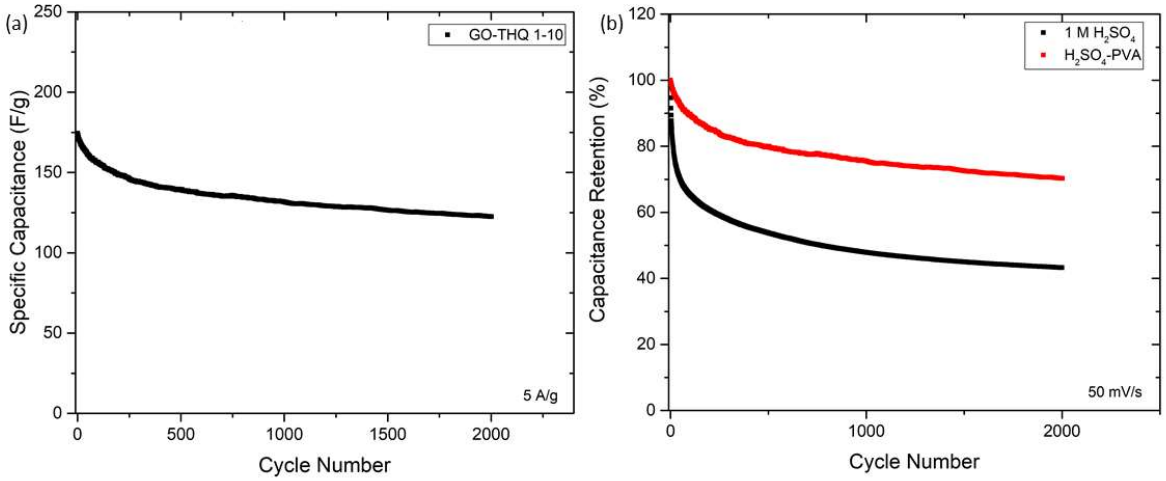

Figure 2.24 (a) Cycling stability test of GO-THQ 1:10 electrode in H_2SO_4-PVA gel electrolyte at 5 A/g for 2000 cycles. (b) Capacitance retention of the GO-THQ 1:10 electrode in 1M H_2SO_4 aqueous electrolyte and H_2SO_4-PVA gel electrolyte.

capacitance retention of the GO-THQ 1:10 electrode during the cycling stability test. By replacing the aqueous electrolyte with the gel electrolyte, the dissolution of the THQ molecule can be reduced. Therefore, the cycling stability of the THQ functionalized graphene electrode can be improved in the gel electrolyte, maintaining 70% of its specific capacitance.

2.4 Conclusion

In this work, the THQ functionalized graphene electrode was synthesized from the mixture of the GO dispersion and THQ at different mass ratios at a low temperature of ~80 ℃ within a short period time of 3 hours under atmosphere condition. The THQ was using as the reducing and functionalization agent simultaneously. The surface chemistry of the graphene electrode can be controlled by the mass ratio between the GO and THQ, which is the concentration of THQ relative to the concentration of the GO dispersion. The 3D functionalized graphene electrodes were characterized with SEM to study the microstructure of the electrode. XPS was also used to study the surface chemistry of the electrodes. The THQ functionalized graphene electrodes were tested in both aqueous electrolyte and gel electrolyte to study the electrochemical performance of the electrode. In the 1 M H_2SO_4 aqueous electrolyte, the THQ functionalized graphene electrode showed a maximum specific capacitance of 409 F/g at the current density of 1 A/g. In the 1 M Li_2SO_4 electrolyte, the electrode also showed outstanding electrochemical performance with a specific capacitance of 125 F/g at the current density of 1 A/g, which makes the THQ functionalized graphene electrode a potential solution to the hybrid supercapacitor capacitive electrode. The cycling stability of the THQ functionalized electrode in aqueous electrolyte is suffering from the dissolution of the THQ molecule into the electrolyte. This could be reduced by replacing the aqueous electrolyte with gel electrolyte. The THQ functionalized graphene electrode was tested in the H_2SO_4-PVA gel electrolyte, giving a specific capacitance of 314 F/g at the current density of 1 A/g. The cycling stability of the THQ functionalized graphene electrode was significantly improved in the gel electrolyte,

giving a capacitance retention over 70% after 2000 cycles at 5 A/g, compared with the ~35% capacitance retention in aqueous electrolytes.

Overall, THQ is an effective additive to the graphene electrode that simplifies the synthesis process of the graphene electrode as well as boosts the electrochemical performance of the graphene electrode in both aqueous and especially in the gel electrolyte. The improvement of the specific capacitance is credited to the porous microstructure and the surface oxygen functional group of the THQ-functionalized electrodes.

CHAPTER 3. QUINONE-GROUP MOLECULES AS FUNCTIONALIZATION AGENTS FOR GRAPHENE ELECTRODES IN SUPERCAPACITORS.

3.1 Introduction

The quinone group molecules have been widely investigated as functionalization agent for carbon-based electrodes including graphene, AC and CNT.[58, 66-68] The quinone group is used for electron and proton storage and exchange during redox cycling. Molecules like hydroquinone (HQ) and p-Benzoquinone (pQ) and 9,10-phenanthrenequinones (PQ) have been used as functionalizing agents for graphene.[69, 70] The quinone molecule functionalized electrode showed outstanding electrochemical performance in supercapacitors due to the faradic reaction between the electrolyte and the carbonyl functional group integrated to the surface of the electrode.[60]

In this work, three quinone group molecules, p-xyloquinone (XQ), 2,5-Dihydroxy-1,4-benzoquinone (DHQ) and 2,5-Dimethoxy-1,4-benzoquinone (DMQ) were studied and tested as functionalizing agent for the graphene electrode. The hydrothermal reaction was carried out at 165 ℃ for 16 hours. The H^+ ions released from the water during the hydrothermal reaction reduced the oxygen functional group on the surface of the graphene layer.[49] The quinone group molecules were incorporated onto the surface of the reduced graphene oxide due to the π- π interaction. The mass ratio of the GO and quinone molecule was maintained at 1:1 for all three electrodes. Over these three quinone group molecules functionalized electrode tested, the GO-DHQ electrode showed the best electrochemical performance with a specific capacitance of 511 F/g in 1 M H_2SO_4 aqueous electrolyte at the current density of 1 A/g. It exhibits a unique 3D microstructure that provides short ion transfer distance and direct contact of the electrolyte to both sides of the graphene layer.

The DHQ functionalized graphene electrode also showed great capacitance retention, it stabilized at 90% of the initial capacitance after 2000 cycles of charge-discharge at 50 mV/s. While the DMQ functionalized graphene electrode only maintained ~70% of its capacitance after the cycling stability test.

3.2 Experimental

3.2.1 Preparation of the Graphene Hydrogel

The graphene oxide single layer dispersion (GO) was prepared by oxidation of natural graphite power according to the modified Hummers' method with a concentration of 7 mg/ml.[50] 4.29 ml of the GO suspension was diluted to 15 mL (2 mg/mL) with DI water in glass vials. 2,5-Dihydroxy-1,4-benzoquinone (DHQ, 98% purity, Fisher Chemicals), p-xyloquinone (XQ, TCI chemicals, 98% purity), or 2,5-dimethoxy-1,4-benzoquinone (DMQ, TCI chemicals, 98% purity) was added to the GO suspension at the mass ratio of 1:1. To prepare the GH, the mixture of GO and quinone group molecule was sonicated for 15 mins and then sealed in a Teflon-lined autoclave for a hydrothermal reaction at 165 ℃ for 16 hours. **Figure 3.1a** shows the mixtures of GO and quinone group molecules; **Figure 3.1b** shows the functionalized GHs obtained from the hydrothermal reaction. After the hydrothermal reaction, the GHs were washed with DI water for several times to remove the excess quinone group molecules until the water become completely clear.

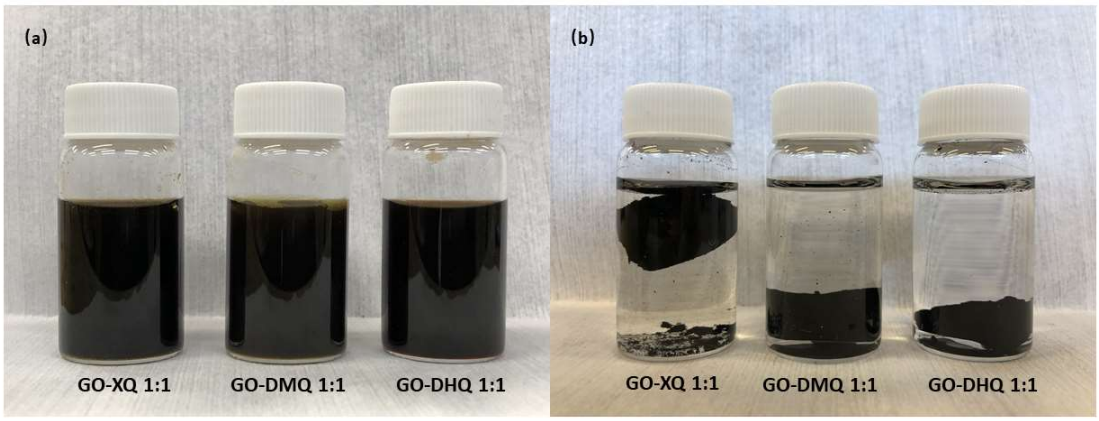

Figure 3.1 (a) GO-XQ 1:1 mixture, GO-DMQ 1:1 mixture and GO-DHQ 1:1 mixture before the hydrothermal reaction. (b) The GO-XQ, GO-DMQ and GO-DHQ graphene hydrogel obtained from the hydrothermal reaction at 165 ℃ for 16 hours.

3.2.2 Prepare the supercapacitor electrodes

The synthesized quinone group molecules functionalized graphene hydrogels were immersed into 1 M aqueous H_2SO_4 electrolyte overnight after washing with DI-water. Then the hydrogel was pressed at 10 kN for 3 mins to form a self-supported thin film with a thickness ranging from 25 to 35 um. The thin film was further cut into multiple electrodes with a diameter of 0.635 cm and a dried mass around 0.52 mg. The dry mass was obtained by parallel measurement, where an electrode with the same mass was washed with water for several times to remove the electrolyte, then dried overnight in the vacuum oven. Similar processes were applied to all three quinone functional functionalized GHs to prepare the supercapacitor electrodes. The detailed information including mass, area, mass loading, thickness and density of the electrodes is given in **Table 2**.

Table 2 Dimensions and specifications of the DMQ functionalized graphene electrode, DHQ functionalized graphene electrodes and XQ functionalized graphene electrode at GO to molecule mass ratio of 1:1.

	Dry mass (mg)	Area (cm^2)	Mass loading (g/cm^2)	Thickness (mm)	Density (g/cm^3)
GO-DMQ 1:1	0.520	0.317	1.642	0.025	0.657
GO-DHQ 1:1	0.450	0.317	1.421	0.025	0.568
GO-XQ 1:1	0.750	0.317	2.368	0.036	0.658

3.2.3 Assemble the supercapacitor

The prepared electrode was used to assemble supercapacitor for the electrochemical tests. Like the previous chapter, the supercapacitor used a symmetric configuration (two electrode system), where no reference electrode was used in this experiment. Two pieces of Platinum foils were used as the current collector of the supercapacitor. The electrode was placed onto the Platinum foil and separated by the Celgard 3510 polypropylene membrane. The two current collectors were pressed together by two glass plates. The assembled cell was immersed into the electrolyte for the Cycle Voltammetry (CV), charge-discharge test. Instead of immersing the cell into the electrolyte, the cell was wrapped by the parafilm after adding electrolyte into the cell for the cycling stability test to reduce the dissolution of the quinone molecules.

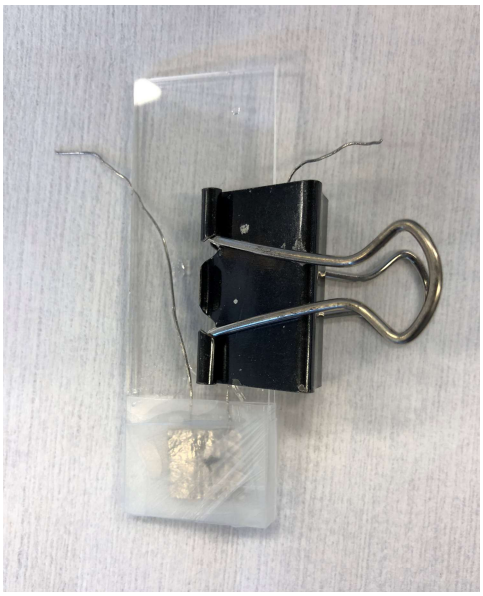

Figure 3.2 Experimental setup for the cycling stability test. The cell was assembled and then wrapped with parafilm to avoid evaporation of the electrolyte. Instead of immersing the electrode into excess amount of electrolyte, this experimental setup is helpful to improve the cycling stability of the electrode in aqueous electrolyte.

3.3 Result and Discussion

3.3.1 Characterization

The prepared functionalized graphene hydrogels were freeze-dried with the Labconco Freezone 2.5L benchtop freeze dryer. The Scanning Electron Microscope (SEM) images of the functionalized graphene aerogel with different molecules were taken with Hitachi SU8010 SEM at 3 KV. The images are shown in **Figure 3.3.**

Figure 3.3a shows the microstructure of the XQ functionalized graphene, which is an interconnected porous structure. The microstructure of the DMQ functionalized graphene shown in **Figure 3.3b** is similar to the microstructure of the XQ functionalized graphene but more porous. However, the microstructure of the DHQ functionalized graphene is clearly different from **Figure 3.3a** and **Figure 3.3b**. Instead of the porous structure, it consists of large graphene layers with rough surfaces. The surface area of the characterized materials needs further study with the gas absorption test to determine which graphene aerogel has the maximum specific surface area. The unique microstructure of the GO-DHQ electrode gives a direct contact with the electrolyte, which shortens the time for ion

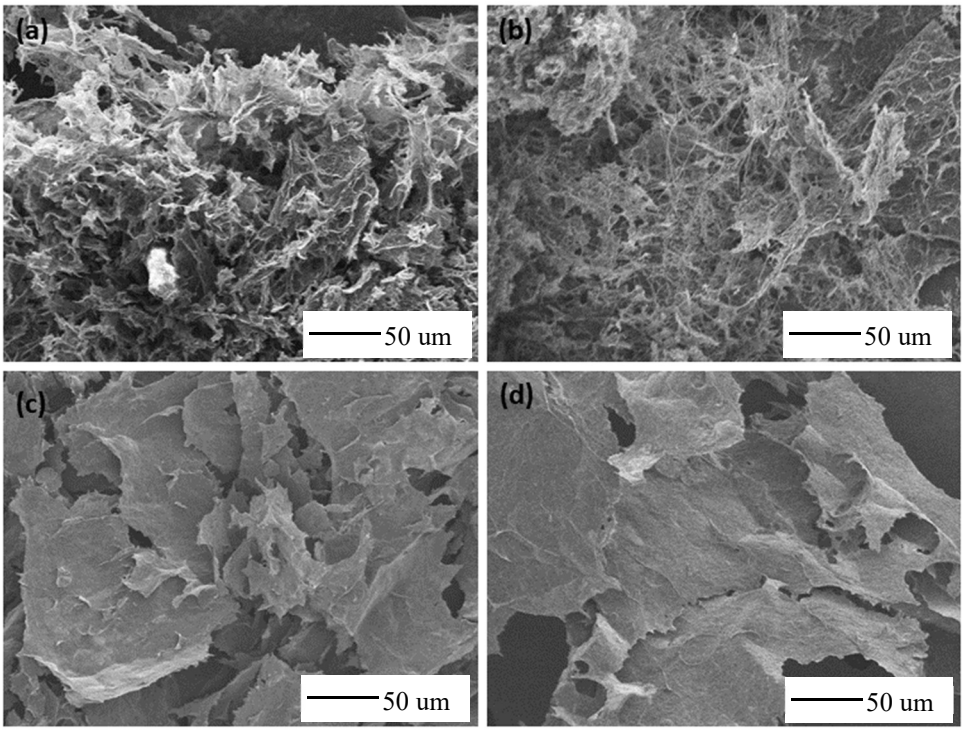

Figure 3.3 Low-magnification Scanning Electron Microscope (SEM) images of the quinone group molecule functionalized graphene aerogels. (a) XQ functionalized graphene aerogel, (b) DMQ functionalized graphene aerogel, (c) and (d) DHQ functionalized graphene aerogel.

penetration and provides higher capacitance at high current density. The gap between the graphene layers make both side of the graphene layers accessible to the electrolyte, which further increase the electrochemical performance of the DHQ functionalized graphene electrode.

The surface chemistry of the synthesized aerogels was characterized using the Thermo K-alpha X-ray Photoelectron Spectroscopy (XPS). **Figure 3.4** is the XPS wide scan survey of the quinone group molecules functionalized electrodes. The GO-DHQ 1:1 electrode showed the highest oxygen to carbon ratio compared with the GO-XQ 1:1 electrode and the GO-DMQ 1:1 electrode. **Figure 3.5** exhibits the C1s spectra of the electrodes. Interestingly, the GO-DMQ 1:1 electrode showed a slightly higher carbonyl group (C=O) peak compared to the GO-DHQ electrode and GO-XQ electrode. The reason for the phenomenon may relate to the methoxy group, methyl group and hydroxy group in the molecule, which is currently unclear. The chemical mechanism behind this still needs further study.

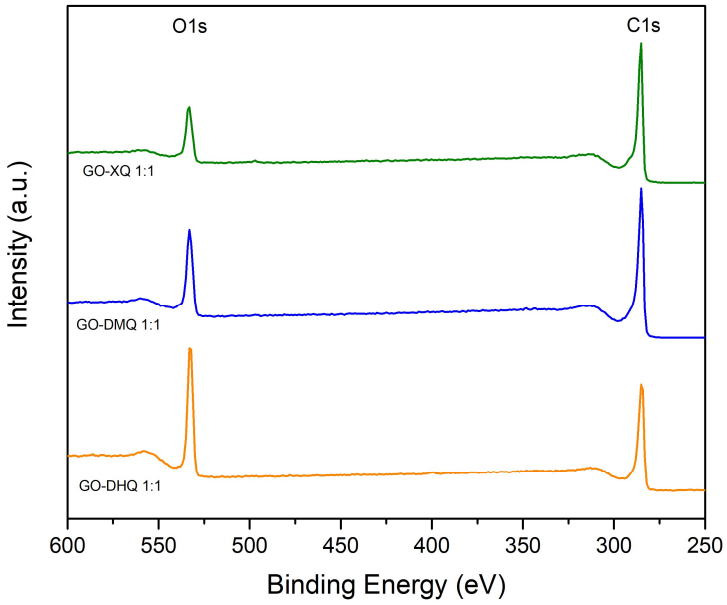

Figure 3.4 XPS wide scan survey of the quinone group molecules functionalized electrodes at 1:1 mass ratio. (top) GO-XQ 1:1 electrode, (middle) GO-DMQ 1:1 electrode, and (bottom) GO-DHQ 1:1 electrode.

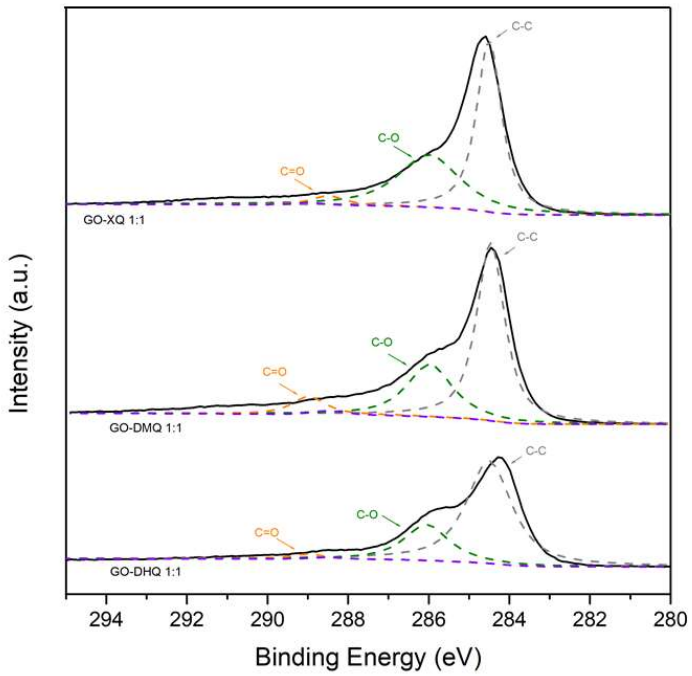

Figure 3.5 XPS C1s spectra of the quinone group molecules functionalized electrodes at 1:1 mass ratio. (top) GO-XQ 1:1 electrode, (middle) GO-DMQ 1:1 electrode, and (bottom) GO-DHQ 1:1 electrode.

3.3.2 Electrochemical tests in 1M H_2SO_4 aqueous electrolyte

The electrodes were synthesized under exact same condition (165 ℃ for 16 hours) and same concentration ratio between the GO and quinone group molecules (1:1). The self-assembled quinone group molecule containing graphene hydrogel was formed due to the reduction of the H^+ and the hydrophobic character.[71] The quinone group molecules were attached to the graphene electrode with the π-π stacking interactions with the graphene sheets and were used as the functionalization agent to provide redox-active functionalities. The other function of the quinone group molecule is avoiding the aggregation of the graphene sheet and providing ion transport channels. The different functional groups incorporated onto the surface of the graphene can provide different microstructures and electrochemical performance.

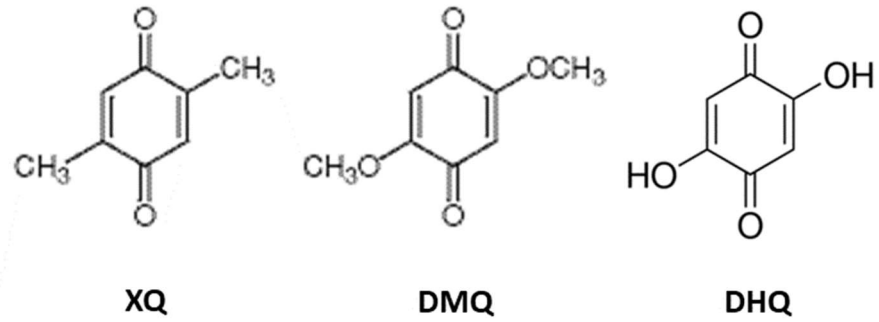

Figure 3.6 Two-dimensional structures of quinone group molecules.

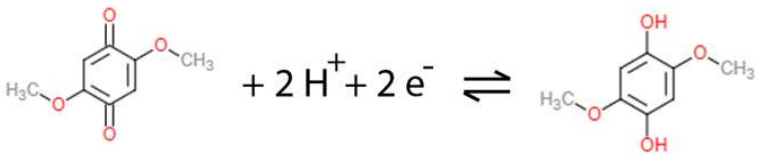

Figure 3.7 Redox charge storage mechanism of the GO-DMQ electrode.

The Redox charge storage mechanism of the DMQ functionalized graphene electrodes are shown as **Figure 3.7**. The XQ and DHQ functionalized graphene electrodes have the same redox charge storage mechanism as DMQ. [64]

The steady-state CV scans at 5 mV/s of the rGO electrode and the quinone group molecule functionalized electrodes are shown in **Figure 3.8**. All three electrodes showed reversible redox peak within 0.1 - 0.4 V and 0.7 – 0.9 V. The CV scans of the DHQ functionalized graphene electrode showed the maximum redox peak followed by the DMQ functionalized electrode and the XQ functionalized electrode showed minimum redox peak among the three electrodes. The CV scan of rGO electrode was also plotted on **Figure 3.8** as a reference for the quinone group functionalized electrodes. The rGO electrode has an ideal rectangular CV shape, indicating a pure EDLC charge storage mechanism. The specific capacitance of the electrodes was estimated using **Equation 2**, where the XQ functionalized graphene electrode has the lowest specific capacitance of ~158.42 F/g compared to ~211.02 F/g for the rGO electrode. The DHQ functionalized graphene electrode showed the highest specific capacitance of 505.51 F/g and the DMQ has a specific capacitance of 316.94 F/g at 5 mV/s.

The CV scans of the rGO electrode and the functionalized electrodes at scan rate from 5 mV/s to 100 mV/s are shown in **Figure 3.9**. As the scan rate increased from 50 mV/s to 100 mV/s, the contribution of pseudocapacitance decreased indicated by smaller redox peaks and the deformation of the scan curve. **Figure 3.9 (d)** shows the comparison of CV scans of the functionalized graphene electrodes and the rGO electrode. At the scan rate of 50 mV/s, there were obvious redox peaks on the CV scans for the DHQ functionalized electrode. This is due to the robust incorporation of the quinone

functionalization group onto the surface of the graphene sheets. The area under the DHQ functionalized electrode CV scan is about 100% larger than the area under the CV scan of the rGO electrode at the scan rate of 50 mV/s, which qualitatively indicates a greater

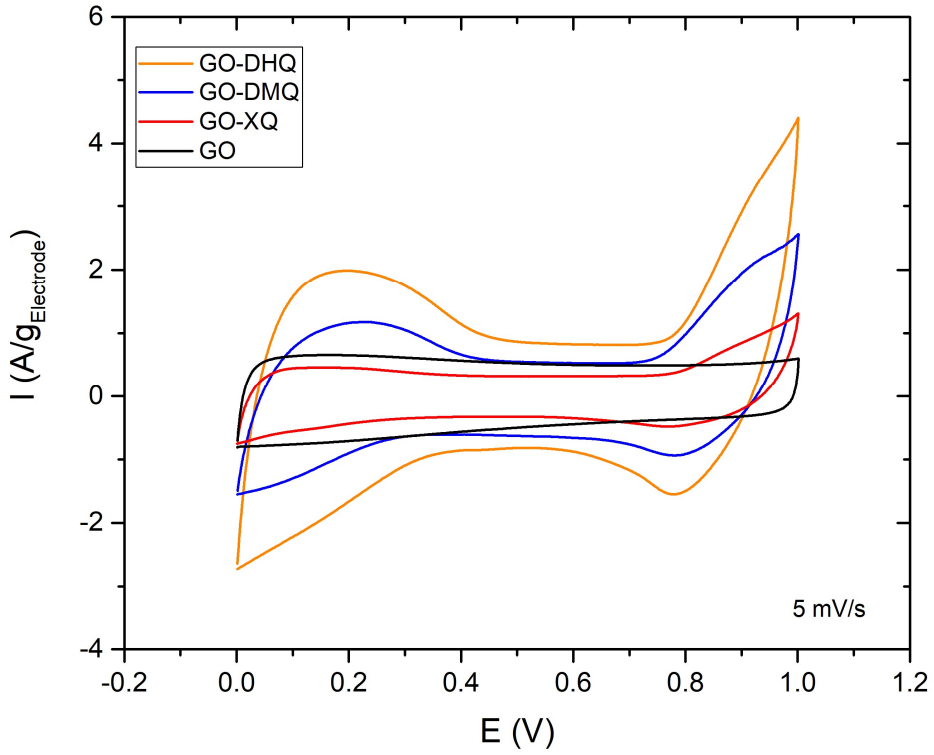

Figure 3.8 Comparison of the steady-state CV scans of the rGO electrode and quinone group molecule functionalized graphene electrodes in 1 M H_2SO_4 electrolyte at scan rate of 5 mV/s, the voltage window of the CV is 0 – 1 V.

specific capacitance. However, the specific capacitance of GO-XQ electrode showed lower specific capacitance than the rGO electrode at 50 mV/s based on the area under the CV scans.

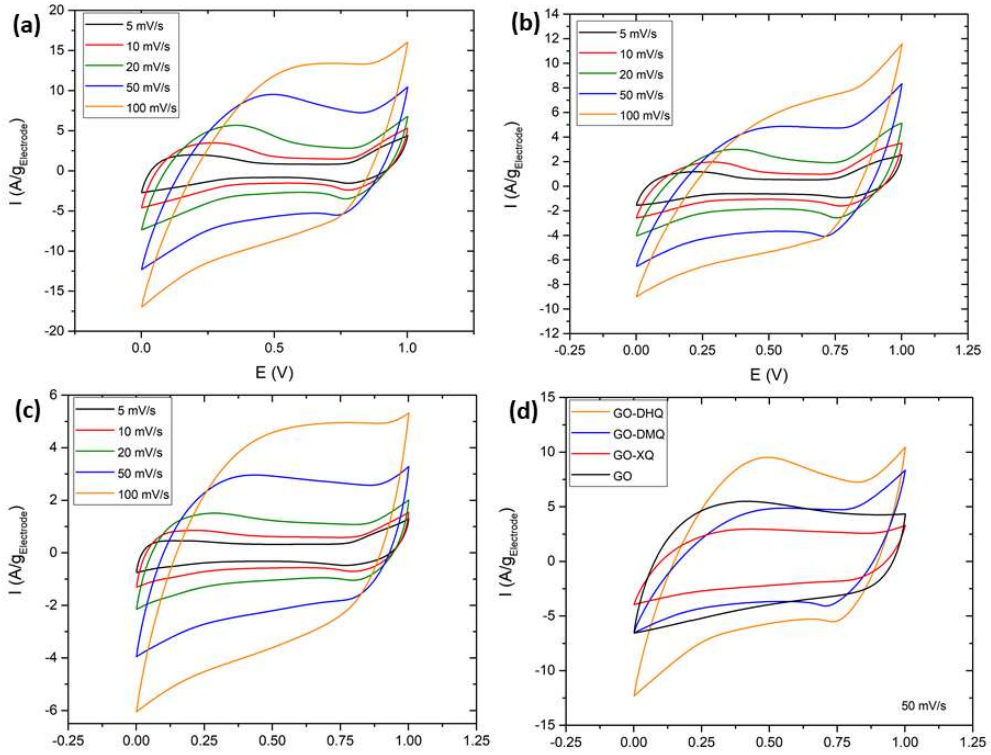

Figure 3.9 Steady-state CV scans at different scan rates, 5, 10, 20, 50 and 100 mV/s for quinone group molecule functionalized graphene electrodes in 1 M H_2SO_4 electrolyte at 0-1 V. (a) GO-DHQ 1:1 electrode, (b) GO-DMQ 1:1 electrode, (c) GO-XQ 1:1 electrode. (d) Comparison of steady-state CV scans of rGO electrode and quinone group functionalized electrodes at 50 mV/s scan rate, voltage window 0-1 V.

The galvanostatic charge-discharge test of the tested electrodes at the current density of 1 A/g is shown in **Figure 3.10**, where both the GO-DHQ electrode and the GO-DHQ electrode showed reversible redox reaction on the curve. Compared with the ideal triangular shape of the rGO electrode charge-discharge curve, the GO-DHQ and GO-DMQ curves confirmed the synergistic contribution of EDLC and pseudocapacitance since the galvanostatic charge-discharge curve of the functionalized electrode exhibited different slopes between 0.2 to 0.5 V and 0.75 to 0.9 V. The galvanostatic charge-discharge test was conducted at 0.5 A/g, 1 A/g, 2 A/g, 5 A/g and 10 A/g.

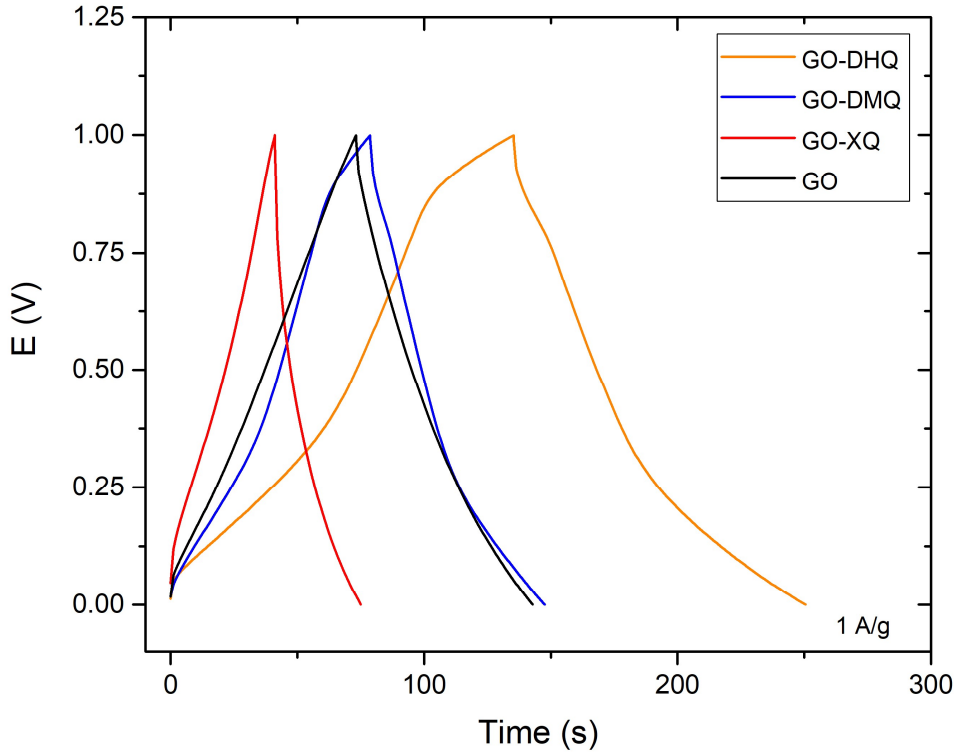

Figure 3.10 Galvanostatic charge-discharge curves of rGO electrode, GO-DHQ 1:1 electrode, GO-DMQ 1:1 electrode and GO-XQ 1:1 electrode in 1M H_2SO_4-aqueous electrolyte at current density of 1 A/g.

The current density dependent specific capacitance was estimated with **Equation 3**. **Figure 3.11** presents the specific capacitance of the electrodes at 0.5 A/g, 1 A/g, 2 A/g, 5 A/g and 10 A/g, where the GO-DHQ 1:1 electrode showed highest specific capacitance at all current densities. At 0.5 A/g and 1 A/g, the GO-DHQ 1:1 electrode showed an excellent specific capacitance of 563.83 F/g and 511.11 F/g. Even at the high current density of 10 A/g, the GO-DHQ 1:1 electrode has the specific capacitance of 236.36 F/g, which is almost three times higher than the 84.29 F/g for the rGO electrode. This is due to the faradic reaction between the carbonyl functional group incorporated to the surface of the graphene layers. The unique microstructure of the GO-DHQ electrode also contributes to the excellent specific capacitance at high current densities. The SEM image of the GO-DHQ

1:1 electrode demonstrate a microstructure of large piece of graphene layer with rough surfaces and large gap between graphene layers. The microstructure provides instant contact of the electrolyte with the active material in the electrode. It allows the electrolyte ions contact both sides of the graphene layer and provides short ion transfer distance, which gives a high specific capacitance at high current density.

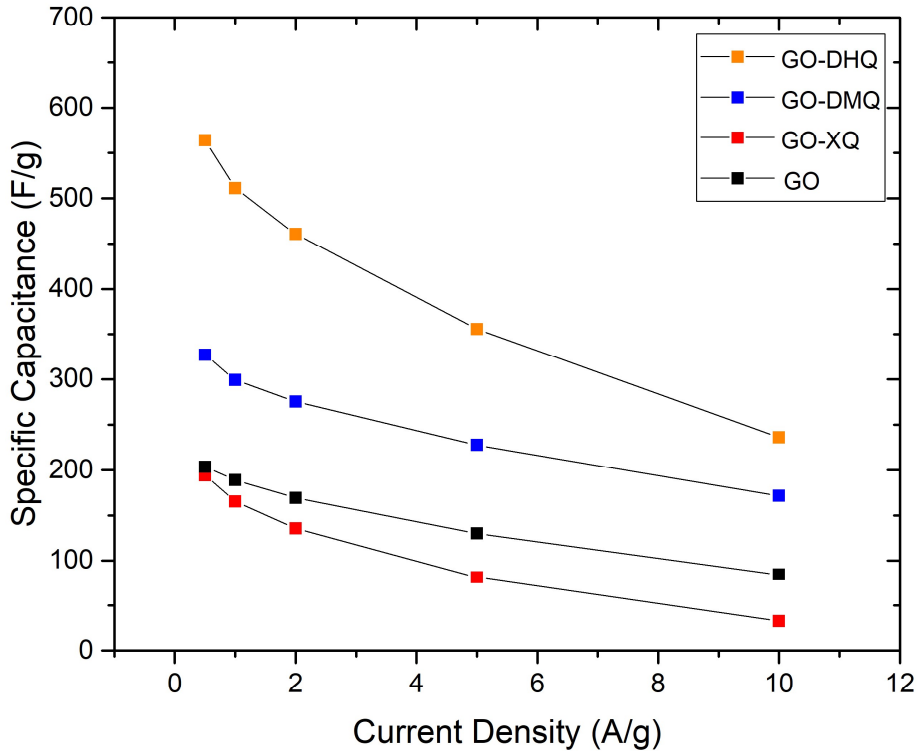

Figure 3.11 Galvanostatic specific capacitance of rGO electrode, GO-DHQ 1:1 electrode, GO-DMQ 1:1 electrode and GO-XQ 1:1 electrode at current density of 1, 2, 5 and 10 A/g.

Figure 3.12 shows the cycling stability of the quinone group molecules functionalized electrodes from 1 to 2000 cycles at a scan rate of 50 mV/s. The cycling stabilities of the functionalized graphene electrodes were compared with the cycling stability of rGO electrode. The GO-DHQ 1:1 electrode has the best cycling stability among

all the tested electrodes with the highest capacitance retention of ~90% after 2000 cycles at 50 mV/s. The GO-XQ 1:1 electrode and the rGO electrode both have ~85% capacitance retention after 2000 cycles. The GO-DMQ electrode showed the worst cycling stability, stabilized at ~70% capacitance retention. The increase in the cycling stability of quinone group molecules functionalized electrode is may be due to the hydrothermal reaction at high temperature (165 ℃) and long duration (16 hours), which can facilitate the stacking of the graphene sheets. The redox-active molecules may be inserted between the graphene sheets during the hydrothermal reaction. As the redox-active molecules were strongly integrated into the graphene electrode, the dissolution of the functionalization groups was significantly decreased during the cycling stability test.[64]

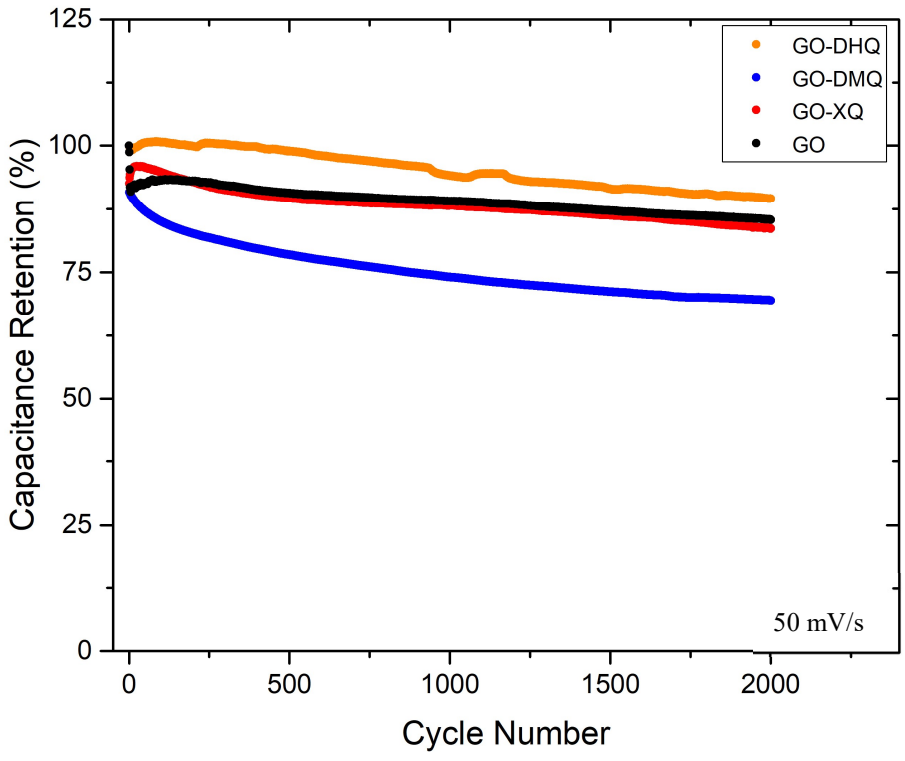

Figure 3.12 Cycling stability test of quinone group molecules functionalized electrode and rGO electrode in 1 M H_2SO_4 aqueous electrolyte at scan rate of 50 mV/s for 2000 cycles.

3.4 Conclusion

In this work, p-xyloquinone (XQ), 2,5-dihydroxy-1,4-benzoquinone (DHQ) and 2,5-dimethoxy-1,4-benzoquinone (DMQ) were used as functionalization molecules for the graphene electrode. The mixture of 2 mg/ml GO suspension and functionalization molecule at the mass ratio of 1:1 was put into a Teflon-lined autoclave for a hydrothermal reaction at 165 ℃ for 16 hours. Part of the obtained graphene hydrogels were pressed and cutting into electrodes for electrochemical tests, while the rest of the obtained graphene hydrogels were freeze-dried and characterized with SEM and XPS.

The GO-THQ has a unique microstructure of large pieces of functionalized graphene layers with rough surfaces. This provides a direct contact of the electrolyte and both sides of the graphene layers. The XPS result indicates the GO-DHQ 1:1 electrode has the largest Carbon to Oxygen ratio due to the integrated oxygen functional groups.

The quinone group functionalized electrodes exhibits the existence of pseudocapacitance. The DHQ functionalized graphene electrode showed the best electrochemical performance, a specific capacitance at ~511 F/g at the current density of 1 A/g. At the high current density of 10 A/g, the GO-DHQ 1:1 electrode maintained a specific capacitance of ~236 F/g, which is almost 3 times higher than the specific capacitance of the rGO electrode. The excellent electrochemical performance of the GO-DHQ 1:1 electrode is due to the joint contribution of the unique 3D microstructure and the surface chemistry. In terms of cycling stability, the GO-DHQ 1:1 electrode stabilized at ~90% capacitance retention after 2000 cycles of scan at 50 mV/s. While the GO-DMQ only maintained ~70% of its initial capacitance after 2000 cycles. The reason for the improved

cycling stability may be due to the elevated reaction temperature and reaction time of the hydrothermal reaction, which can facilitate the integration of the oxygen functional groups between the graphene sheets.

CHAPTER 4. CONCLUSION AND OUTLOOK

In the first part of this thesis, the charge storage mechanism and electrochemical performance of redox-active organic molecule (THQ) functionalized graphene electrode in different electrolytes were investigated. The reduced graphene electrode was also tested as the reference to the THQ functionalized graphene electrode. In 1 M H_2SO_4 aqueous electrolyte, the THQ functionalized graphene electrode showed specific capacitance of ~409 F/g at 1 A/g compared to ~189 F/g of the rGO electrode. The THQ functionalized graphene electrode suffers from the dissolution of the molecules into the aqueous electrolyte, maintained only 35% of its original capacitance after 5000 cycles at 5 A/g current density, compared with ~80% of the rGO electrode. In 1 M Li_2SO_4 aqueous electrolyte, the THQ functionalized electrode also showed the great performance (~125 F/g), making it a potential electrode material for the Li-ion hybrid capacitors. The THQ functionalized electrode was also tested in H_2SO_4-PVA gel electrolyte with a specific capacitance of ~315 F/g at 1 A/g. The capacitance retention of the THQ functionalized electrode stabilized at ~80% after 2000 cycles at 5 A/g, increased from 35% in the aqueous electrolyte. The increase in specific capacitance is due to the synergetic contribution of the porous microstructure and the pseudocapacitance of the oxygen functional group. The improved cycling stability in the gel electrode makes the THQ functionalized graphene electrode a promising electrode material for flexible solid-state supercapacitor.

In the second part of this thesis, three quinone group molecules, p-xyloquinone (XQ), 2,5-Dihydroxy-1,4-benzoquinone (DHQ) and 2,5-Dimethoxy-1,4-benzoquinone (DMQ) were used as functionalization agent of the redox-active graphene electrode. The

electrodes were synthesized via hydrothermal reaction at 165 ℃ for 16 hours. DHQ functionalized electrode showed excellent electrochemical performance, 511 F/g at 1 A/g and 236 F/g at 10 A/g, which is almost 3 times higher than the specific capacitance of the rGO electrode. The improvement of the electrochemical performance is credited to the incorporated oxygen functional group and the unique 3D microstructure of the electrode. The interconnected graphene layers provide low internal resistance and the direct contact of the electrolyte with both sides of the functionalized graphene layers provide channels for ion transfer and shorten the ion transfer distance. Due to the high-temperature hydrothermal reaction, the redox-active molecules were robustly integrated to the graphene layers, which greatly improved the cycling stability of the quinone group functionalized graphene electrodes. After 2000 cycles, the GO-DHQ 1:1 electrode stabilized at ~90% of its initial capacitance.

More works have been already scheduled after the completion of this thesis. More characterizations of the electrodes are necessary to determine the specific surface area of the electrodes and the surface chemistry of the electrode after the cycling stability test. The electrode will be synthesized at different mass ratio between the GO and redox-active organic molecule to determine the optimal performance of the electrode. Other synthesis methods of the functionalized electrode will also be tested for the possibility of mass production with lower manufacturing cost. Assembling yarn supercapacitor consist of DHQ functionalized graphene as the power source for wearable devices is also part of the future works.[72-75] Cycling stability of the electrode will be determined for more cycles. The functionalized electrodes will also be tested as Li-ion battery cathodes.[76, 77] More fundamentally investigation related to the roles of the methoxy group, methyl group and

hydroxy group during synthesis process and the electrochemical test will be completed and it will be the critical reason why the GO-DHQ electrode showed better performance compared to the GO-DMQ electrode.

REFERENCES

1. Zhang, L.L. and X.S. Zhao, *Carbon-based materials as supercapacitor electrodes.* Chem Soc Rev, 2009. **38**(9): p. 2520-31.

2. Ruiz, V., et al., *An activated carbon monolith as an electrode material for supercapacitors.* Carbon, 2009. **47**(1): p. 195-200.

3. Zhu, Y., et al., *Carbon-Based Supercapacitors Produced by Activation of Graphene.* Science, 2011. **332**(6037): p. 1537.

4. Futaba, D.N., et al., *Shape-engineerable and highly densely packed single-walled carbon nanotubes and their application as super-capacitor electrodes.* Nat Mater, 2006. **5**(12): p. 987-94.

5. Simon, P., Y. Gogotsi, and B. Dunn, *Where Do Batteries End and Supercapacitors Begin?* Science, 2014. **343**(6176): p. 1210.

6. Wang, G., L. Zhang, and J. Zhang, *A review of electrode materials for electrochemical supercapacitors.* Chem Soc Rev, 2012. **41**(2): p. 797-828.

7. Barré, A., et al., *A review on lithium-ion battery ageing mechanisms and estimations for automotive applications.* Journal of Power Sources, 2013. **241**: p. 680-689.

8. Tarascon, J.M. and M. Armand, *Issues and challenges facing rechargeable lithium batteries.* Nature, 2001. **414**: p. 359.

9. Simon, P. and Y. Gogotsi, *Charge storage mechanism in nanoporous carbons and its consequence for electrical double layer capacitors.* Philosophical Transactions of the Royal Society A: Mathematical, Physical and Engineering Sciences, 2010. **368**(1923): p. 3457-3467.

10. Yoshio, M., R.J. Brodd, and A. Kozawa, *Lithium-ion batteries*. Vol. 1. 2009: Springer.

11. Winter, M. and R.J. Brodd, *What are batteries, fuel cells, and supercapacitors?* 2004, ACS Publications.

12. Shi, H., *Activated carbons and double layer capacitance.* Electrochimica Acta, 1996. **41**(10): p. 1633-1639.

13. Augustyn, V., et al., *High-rate electrochemical energy storage through Li+ intercalation pseudocapacitance.* Nature materials, 2013. **12**(6): p. 518.

14. Lang, X., et al., *Nanoporous metal/oxide hybrid electrodes for electrochemical supercapacitors.* Nature nanotechnology, 2011. **6**(4): p. 232.

15. Peng, C., et al., *Carbon nanotube and conducting polymer composites for supercapacitors.* Progress in Natural science, 2008. **18**(7): p. 777-788.

16. Simon, P. and Y. Gogotsi, *Materials for electrochemical capacitors.* Nature Materials, 2008. **7**: p. 845.

17. Fergus, J.W., *Recent developments in cathode materials for lithium ion batteries.* Journal of Power Sources, 2010. **195**(4): p. 939-954.

18. Kucinskis, G., G. Bajars, and J. Kleperis, *Graphene in lithium ion battery cathode materials: A review.* Journal of Power Sources, 2013. **240**: p. 66-79.

19. Chan, C.K., et al., *High-performance lithium battery anodes using silicon nanowires.* Nature nanotechnology, 2008. **3**(1): p. 31.

20. Yang, M., et al., *Fabrication of High‐Power Li‐Ion Hybrid Supercapacitors by Enhancing the Exterior Surface Charge Storage.* Advanced Energy Materials, 2015. **5**(17): p. 1500550.

21. Dubal, D.P., et al., *Hybrid energy storage: the merging of battery and supercapacitor chemistries.* Chemical Society Reviews, 2015. **44**(7): p. 1777-1790.

22. Kang, Y.J., et al., *All-solid-state flexible supercapacitors based on papers coated with carbon nanotubes and ionic-liquid-based gel electrolytes.* Nanotechnology, 2012. **23**(6): p. 065401.

23. Pech, D., et al., *Ultrahigh-power micrometre-sized supercapacitors based on onion-like carbon.* Nature nanotechnology, 2010. **5**(9): p. 651.

24. Kang, K., et al., *Electrodes with High Power and High Capacity for Rechargeable Lithium Batteries.* Science, 2006. **311**(5763): p. 977-980.

25. Zuo, W., et al., *Battery‐Supercapacitor Hybrid Devices: Recent Progress and Future Prospects.* Advanced Science, 2017. **4**(7): p. 1600539.

26. Naoi, K., et al., *Second generation 'nanohybrid supercapacitor': evolution of capacitive energy storage devices.* Energy & Environmental Science, 2012. **5**(11): p. 9363-9373.

27. Frackowiak, E. and F. Beguin, *Carbon materials for the electrochemical storage of energy in capacitors.* Carbon, 2001. **39**(6): p. 937-950.

28. Li, B., et al., *Nitrogen-doped activated carbon for a high energy hybrid supercapacitor.* Energy & Environmental Science, 2016. **9**(1): p. 102-106.

29. Byon, H.R., et al., *Role of oxygen functional groups in carbon nanotube/graphene freestanding electrodes for high performance lithium batteries.* Advanced functional materials, 2013. **23**(8): p. 1037-1045.

30. Lee, S.W., et al., *High-power lithium batteries from functionalized carbon-nanotube electrodes.* Nature nanotechnology, 2010. **5**(7): p. 531.

31. Yu, A., et al., *Free-standing layer-by-layer hybrid thin film of graphene-MnO2 nanotube as anode for lithium ion batteries.* The Journal of Physical Chemistry Letters, 2011. **2**(15): p. 1855-1860.

32. Hyder, M.N., et al., *Layer-by-layer assembled polyaniline nanofiber/multiwall carbon nanotube thin film electrodes for high-power and high-energy storage applications.* ACS nano, 2011. **5**(11): p. 8552-8561.

33. Kotov, N.A., I. Dekany, and J.H. Fendler, *Layer-by-layer self-assembly of polyelectrolyte-semiconductor nanoparticle composite films.* The Journal of Physical Chemistry, 1995. **99**(35): p. 13065-13069.

34. Aradilla, D., et al., *Novel hybrid micro-supercapacitor based on conducting polymer coated silicon nanowires for electrochemical energy storage.* Rsc Advances, 2014. **4**(50): p. 26462-26467.

35. Wu, Z.-S., et al., *Graphene/metal oxide composite electrode materials for energy storage.* Nano Energy, 2012. **1**(1): p. 107-131.

36. Yu, G., et al., *Enhancing the supercapacitor performance of graphene/MnO2 nanostructured electrodes by conductive wrapping.* Nano letters, 2011. **11**(10): p. 4438-4442.

37. Zhong, C., et al., *A review of electrolyte materials and compositions for electrochemical supercapacitors.* Chemical Society Reviews, 2015. **44**(21): p. 7484-7539.

38. Zhang, K., et al., *Graphene/polyaniline nanofiber composites as supercapacitor electrodes.* Chemistry of Materials, 2010. **22**(4): p. 1392-1401.

39. Armand, M. and J.-M. Tarascon, *Building better batteries.* nature, 2008. **451**(7179): p. 652.

40. Manthiram, A., Y. Fu, and Y.-S. Su, *Challenges and prospects of lithium–sulfur batteries.* Accounts of chemical research, 2012. **46**(5): p. 1125-1134.

41. Manthiram, A., et al., *Rechargeable lithium–sulfur batteries.* Chemical reviews, 2014. **114**(23): p. 11751-11787.

42. Geim, A.K., *Graphene: status and prospects.* science, 2009. **324**(5934): p. 1530-1534.

43. Tang, L., et al., *Preparation, structure, and electrochemical properties of reduced graphene sheet films.* Advanced Functional Materials, 2009. **19**(17): p. 2782-2789.

44. Sun, Y., Q. Wu, and G. Shi, *Graphene based new energy materials.* Energy & Environmental Science, 2011. **4**(4): p. 1113-1132.

45. Liu, N., et al., *One‐step ionic‐liquid‐assisted electrochemical synthesis of ionic‐liquid‐functionalized graphene sheets directly from graphite.* Advanced Functional Materials, 2008. **18**(10): p. 1518-1525.

46. Ramanathan, T., et al., *Functionalized graphene sheets for polymer nanocomposites.* Nature nanotechnology, 2008. **3**(6): p. 327.

47. Xu, Y., et al., *Flexible graphene films via the filtration of water-soluble noncovalent functionalized graphene sheets.* Journal of the American Chemical Society, 2008. **130**(18): p. 5856-5857.

48. Xu, J., et al., *Hierarchical nanocomposites of polyaniline nanowire arrays on graphene oxide sheets with synergistic effect for energy storage.* ACS nano, 2010. **4**(9): p. 5019-5026.

49. Xu, Y., et al., *Self-assembled graphene hydrogel via a one-step hydrothermal process.* ACS nano, 2010. **4**(7): p. 4324-4330.

50. Hummers Jr, W.S. and R.E. Offeman, *Preparation of graphitic oxide.* Journal of the american chemical society, 1958. **80**(6): p. 1339-1339.

51. Zhou, W., et al., *Flexible wire-like all-carbon supercapacitors based on porous core–shell carbon fibers.* Journal of Materials Chemistry A, 2014. **2**(20): p. 7250-7255.

52. Wang, G., et al., *LiCl/PVA gel electrolyte stabilizes vanadium oxide nanowire electrodes for pseudocapacitors.* ACS nano, 2012. **6**(11): p. 10296-10302.

53. Chen, Z., et al., *Three-dimensional flexible and conductive interconnected graphene networks grown by chemical vapour deposition.* Nature materials, 2011. **10**(6): p. 424.

54. Wu, C., et al., *Highly conductive nanocomposites with three‐dimensional, compactly interconnected graphene networks via a self‐assembly process.* Advanced Functional Materials, 2013. **23**(4): p. 506-513.

55. Chen, X.-C., et al., *A graphene-based nanostructure with expanded ion transport channels for high rate Li-ion batteries.* Chemical Communications, 2012. **48**(47): p. 5904-5906.

56. Yang, X., et al., *Liquid-Mediated Dense Integration of Graphene Materials for Compact Capacitive Energy Storage.* Science, 2013. **341**(6145): p. 534-537.

57. Stoller, M.D., et al., *Graphene-based ultracapacitors.* Nano letters, 2008. **8**(10): p. 3498-3502.

58. Xu, Y., et al., *Functionalized Graphene Hydrogel‐Based High‐Performance Supercapacitors.* Advanced Materials, 2013. **25**(40): p. 5779-5784.

59. Liu, T., et al., *Self-assembled, redox-active graphene electrodes for high-performance energy storage devices.* The journal of physical chemistry letters, 2014. **5**(24): p. 4324-4330.

60. Anjos, D.M., et al., *Pseudocapacitance and performance stability of quinone-coated carbon onions.* Nano Energy, 2013. **2**(5): p. 702-712.

61. Cheng, Y., et al., *Flexible asymmetric supercapacitors with high energy and high power density in aqueous electrolytes.* Nanoscale, 2013. **5**(3): p. 1067-1073.

62. Wei, L., et al., *Hydrothermal carbonization of abundant renewable natural organic chemicals for high‐performance supercapacitor electrodes.* Advanced Energy Materials, 2011. **1**(3): p. 356-361.

63. Quan, M., et al., *Voltammetry of quinones in unbuffered aqueous solution: reassessing the roles of proton transfer and hydrogen bonding in the aqueous electrochemistry of quinones.* Journal of the American Chemical Society, 2007. **129**(42): p. 12847-12856.

64. Boota, M., et al., *Pseudocapacitance and excellent cyclability of 2,5-dimethoxy-1,4-benzoquinone on graphene.* Energy & Environmental Science, 2016. **9**(8): p. 2586-2594.

65. Senoh, H., et al., *A two-compartment cell for using soluble benzoquinone derivatives as active materials in lithium secondary batteries.* Electrochimica Acta, 2011. **56**(27): p. 10145-10150.

66. Velasco-Santos, C., et al., *Improvement of thermal and mechanical properties of carbon nanotube composites through chemical functionalization.* Chemistry of materials, 2003. **15**(23): p. 4470-4475.

67. Qie, L., et al., *Synthesis of functionalized 3D hierarchical porous carbon for high-performance supercapacitors.* Energy & Environmental Science, 2013. **6**(8): p. 2497-2504.

68. Jaffe, A., A. Saldivar Valdes, and H.I. Karunadasa, *Quinone-functionalized carbon black cathodes for lithium batteries with high power densities.* Chemistry of Materials, 2015. **27**(10): p. 3568-3571.

69. Chen, D., H. Feng, and J. Li, *Graphene oxide: preparation, functionalization, and electrochemical applications.* Chemical reviews, 2012. **112**(11): p. 6027-6053.

70. Wu, M., et al., *Hydroxyl-decorated graphene systems as candidates for organic metal-free ferroelectrics, multiferroics, and high-performance proton battery cathode materials.* Physical Review B, 2013. **87**(8): p. 081406.

71. Xu, Y., G. Shi, and X. Duan, *Self-Assembled Three-Dimensional Graphene Macrostructures: Synthesis and Applications in Supercapacitors.* Accounts of Chemical Research, 2015. **48**(6): p. 1666-1675.

72. Lee, J.A., et al., *Ultrafast charge and discharge biscrolled yarn supercapacitors for textiles and microdevices.* Nature communications, 2013. **4**: p. 1970.

73. Wang, K., et al., *High‐performance two‐ply yarn supercapacitors based on carbon nanotubes and polyaniline nanowire arrays.* Advanced materials, 2013. **25**(10): p. 1494-1498.

74. Kou, L., et al., *Coaxial wet-spun yarn supercapacitors for high-energy density and safe wearable electronics.* Nature communications, 2014. **5**: p. 3754.

75. Pu, X., et al., *Wearable self‐charging power textile based on flexible yarn supercapacitors and fabric nanogenerators*. Advanced Materials, 2016. **28**(1): p. 98-105.

76. Jang, B.Z., et al., *Graphene surface-enabled lithium ion-exchanging cells: next-generation high-power energy storage devices.* Nano letters, 2011. **11**(9): p. 3785-3791.

77. Rong, J., et al., *Solution ionic strength engineering as a generic strategy to coat graphene oxide (GO) on various functional particles and its application in high-performance lithium–sulfur (Li–S) batteries.* Nano letters, 2013. **14**(2): p. 473-479.